Atacama
Large
Millimeter
Array

How To Holography

ALMA-90.03.00.00-00x-A-HOW

2006–11–27

HowTo Document

Jeff Mangum, Darrel Emerson, & Robert Lucas

Change Record

Revision	Date	Author	Section/ Page affected	Remarks
1	2006-11-06	Jeff Mangum	All	Initial Draft
2	2006-11-22	Jeff Mangum	All	Updated M&C section and added some appendices
3	2006-11-27	Jeff Mangum	All	Added holography transmitter block diagram

`$Id: HolographyHowTo.tex,v 1.3 2006/11/27 15:19:33 jmangum Exp $`

Contents

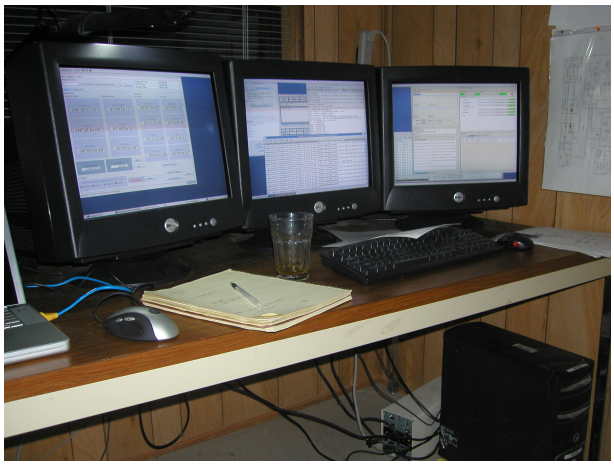

Figure 1: Console1 in the ATF Control Room.

1 Caveats

— This document is meant to be an overview for the "holographer". Its purpose is to give the holographer a single reference for all things holography. More detailed documentation on the monitor and control system can be found elsewhere (*c.f.*[Shepherd (2006)]).
— The GUI-based monitor and control environment is somewhat complicated at the moment. Hopefully, we have provided a path through this maze.
— Updated information on system status, documentation, maps, and trouble shooting tips can be found at *https://wikio.nrao.edu/bin/view/Main/AlmaHolography*.

As the intent of this document is to give a detailed description of the collection, analysis, and theory behind the holography system to the user we have opted to first describe how a holography map is acquired. The ALMA holography system includes two major components: the ALMA Monitor and Control System and the holography hardware. User descriptions of these two systems are described below.

2 The ALMA Monitor and Control System

2.1 Monitor and Control System Startup

— Turn on the Antenna: The antenna to be measured needs to be turned-on and operational. See [Shepherd (2006)] for a description of the antenna START/STOP procedures.
— Start M&C Processes on console1[1]: The control computer at the ATF is "console1", which is the three monitor system in the ATF Control Room (Figure 1).
  — **Log onto console1:** You should log in as yourself, as all monitor and control applications are designed to be used from each user account.
  — **Start the Operator MasterClient (OMC):**

[1]Formerly called "golum" until standard ALMA naming convention took over.

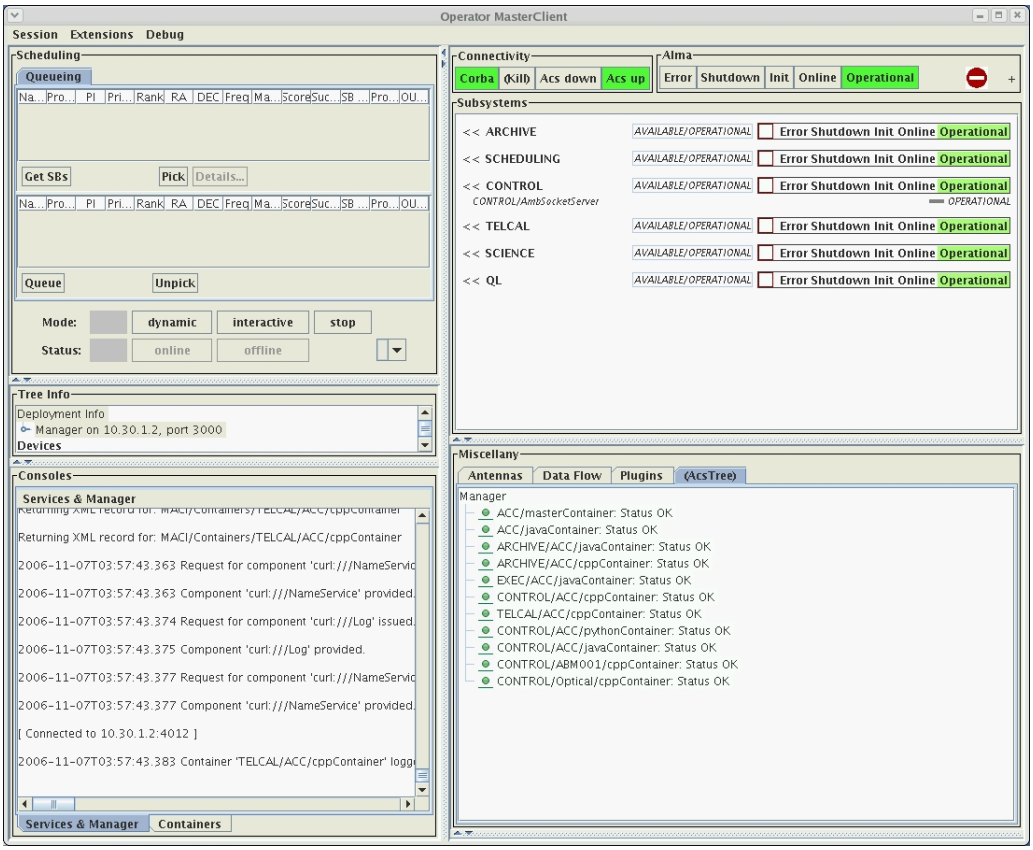

Figure 2: Operator MasterClient GUI.

- *Start an Xterm*
- *Type the command "runOMC":* OMC is your interface to the real-time system (*e.g.* ACC, ABM, *etc.*.).
- *Click "Acs Up" on the OMC GUI "Connectivity" Tab:* This will start up the various M&C "containers". Wait until all container indicators in the "Miscellany" tab turn green.
- *Click "Operational"on the OMC GUI "Alma" Tab:* This will turn the various M&C processes from "shutdown" to "operational". See Figure 2.

— **Start the Scheduling Panel GUI:**

- *Start an Xterm (or open a new tab on your existing Xterm)*
- *Type the command "runSchedulingPanel":* When the GUI starts take a deep breath and follow the incredible and unnecessarily complicated sequence:
  - **Select "Create Array" in the Start Schedulers area of the Main tab**
  - **Select the "CONTROL/ALMA01" antenna and use the arrows to move it into the right list**
  - **Select "Create"**

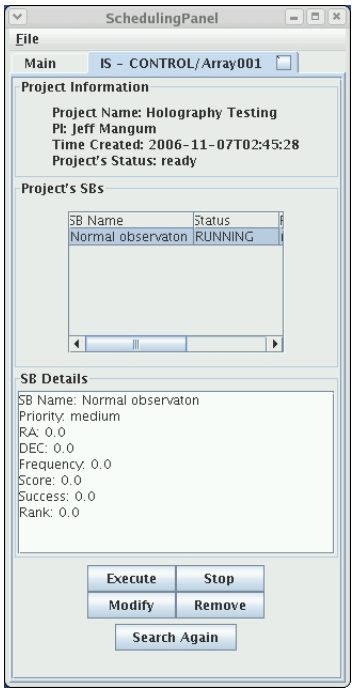

Figure 3: SchedulingPanel GUI.

- **Select "Interactive":** A new tab will appear.
- **Select "CONTROL/Array001":** From the list.
- **Select "Select"**
- **Select the "IS – CONTROL/Array001" tab near the top of the GUI**
- **Select "Search"**
- **Select your SB (called "Project Name":** From the "Projects" box.
- **Select "Select"**
- **Select your SB from the "Project SBs" list box**
- **Select "Execute"**

After this sequence you should see your SB start in the "Data Flow" tab of the "Miscellany" section of the OMC. You will also have a severe case of carpal tunnel syndrome. See Figure 3.

- **Start the Antenna Mount GUI:**
  - *Start an Xterm (or open a new tab on your existing X-term)*
  - *Type the command "mountGUI":* When the GUI starts go to the unnamed pull-down menu near the top of the GUI and change the "none" selection to "CONTROL/ALMA01/MountController". You should see the position information update to the current VertexRSI antenna status. See Figure 4.
- **Start the ALMA OT:**
  - *Start an Xterm (or open a new tab on your existing X-term)*
  - *Type "ssh acc.atf.nrao.edu":* For now, the OT must be run from the ACC computer.

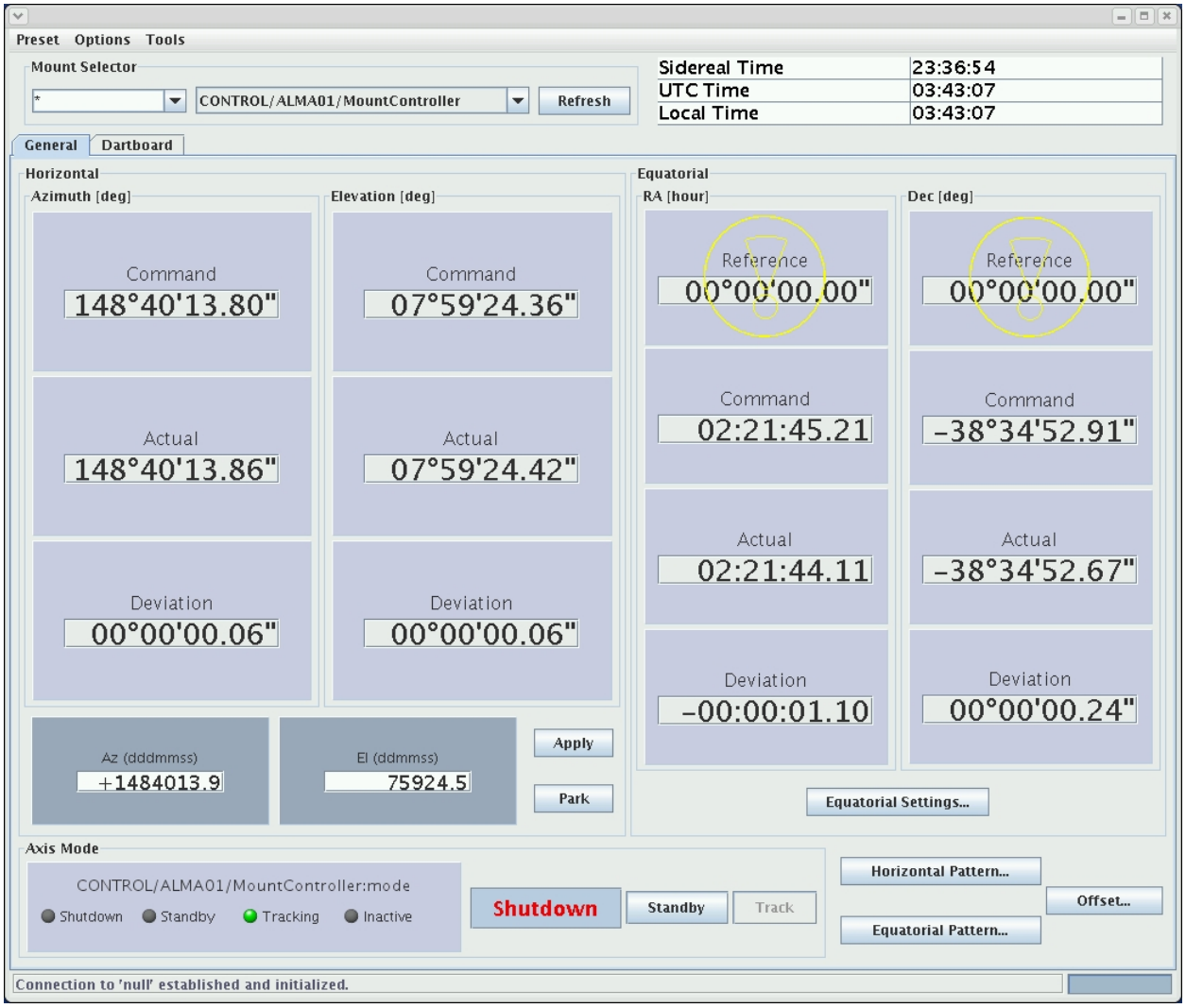

Figure 4: Antenna Mount GUI.

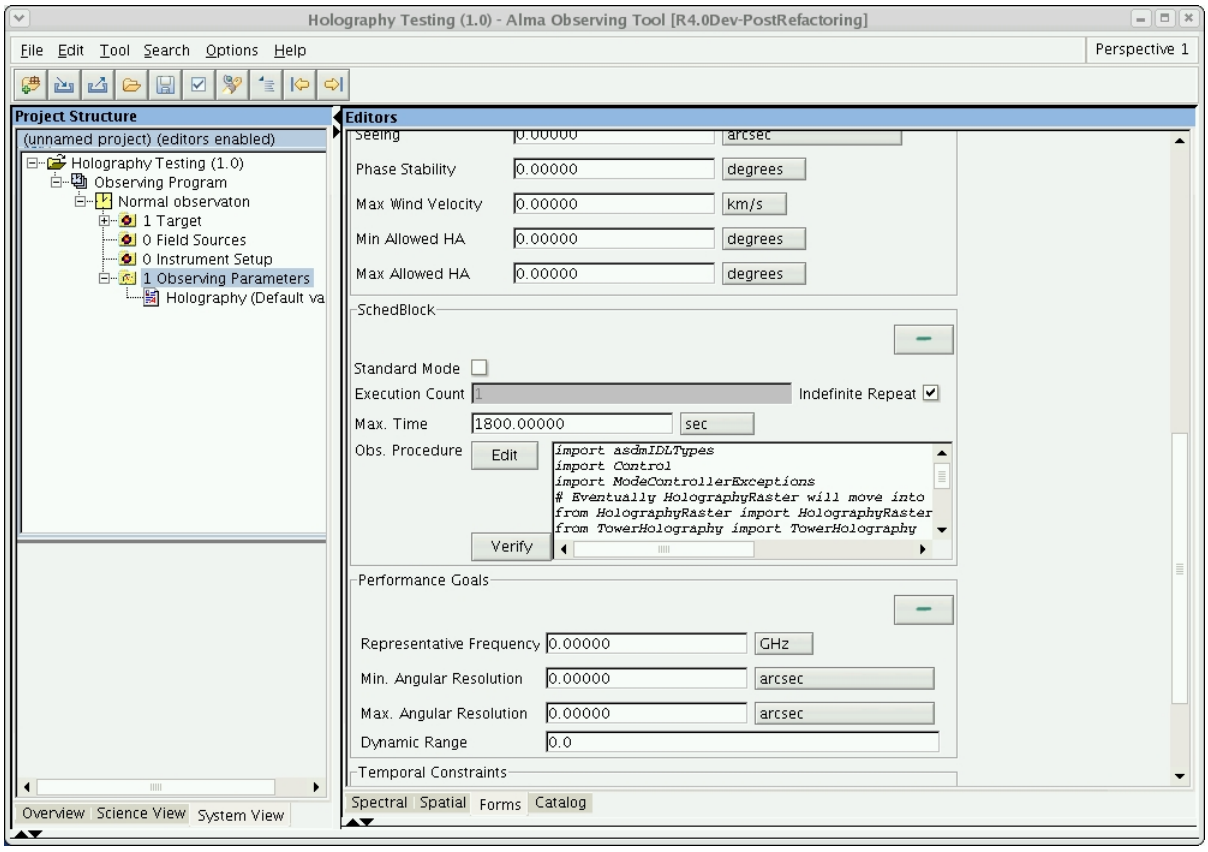

Figure 5: ALMA OT GUI.

- *Type the command "ALMA-OT":* When the GUI starts:
  - *Select "File → Open → Show All"*
  - *Select the project (SB) you want to edit*
  - *Select "Open"*
  - *Navigate through the "Project Structure" until you get to "Observing Parameters"*
  - *Scroll down to "Observing Procedure" and select "Edit":* Edit your script as necessary.
  - *Select "File → Submit" to save your SB:* Your SB will now appear in the SchedulingPanel ready for use.

  See Figure 5.

At this point you should have one or more Xterms with perhaps individual tabs for each of the three applications started above. It is convenient to keep these Xterms/tabs running as one must frequently restart the M&C system. See Figure 6 for an example Xterm layout.

- Start the "ATF Log Viewer" on console1: Most people know this as a "terminal". We need to use the following "traditional" log viewing means as the "jlog" application is...well...not ready for prime-time.
  - *Start a new Xterm*

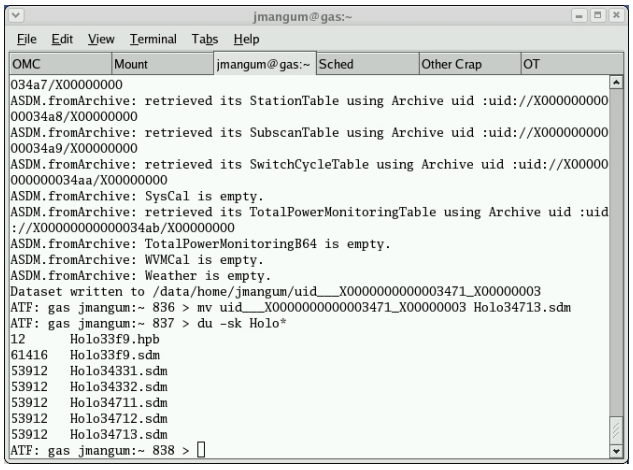

Figure 6: Sample Xterm layout.

- *Type "j̃mangum/Apps/logshow ?":* This will give you a listing of command options for this little log file "viewer".
- *Type "j̃mangum/Apps/logshow p":* To get a row-by-row listing of your map's progress.
- *Open a new tab in the current Xterm*
- *Type "˜jmangum/Apps/logshow c":* To get a more cryptic listing of the detailed sample messages for each row of your map.[2]
- *Type "˜jmangum/Apps/lowshow i":* To get a listing of each UID identifier needed as input to asdmExport. See Figure 7.

— When your SB finishes export the ASDM information to CLIC format:
- **Open an Xterm or another tab**
- **Type "asdmExport uid://X000000000000nnnn/X0000000n":** Where "nnnn" is a number/letter sequence and n is a version number. You can figure out what this number is for your SB by several means, but I find the most useful way is to use "logshow i" and cut-and-paste this ridiculously long string. Once asdmExport finishes you should probably rename the resultant ASDM directory to something sensible. I have been simply stripping-off the excessive 0's and X's and using names like Holo345d1.sdm where "nnnn" was "345d" and "n" was "1".

You are now ready to run CLIC to analyze your map.

2.2 Monitor and Control System Shutdown

— Exit MountGUI: Click on the 'x' in upper right of the window. Note that will make the GUI go away but will not stop the process (a known bug). To regain control of the X-term type 'control-C'.
— Shut Down OMC Processes:
- **Select "Shutdown" in the OMC GUI:** This will send the various OMC processes from "Operational" to "Shutdown". This will take a few moments.

[2]This option really doesn't work right yet.

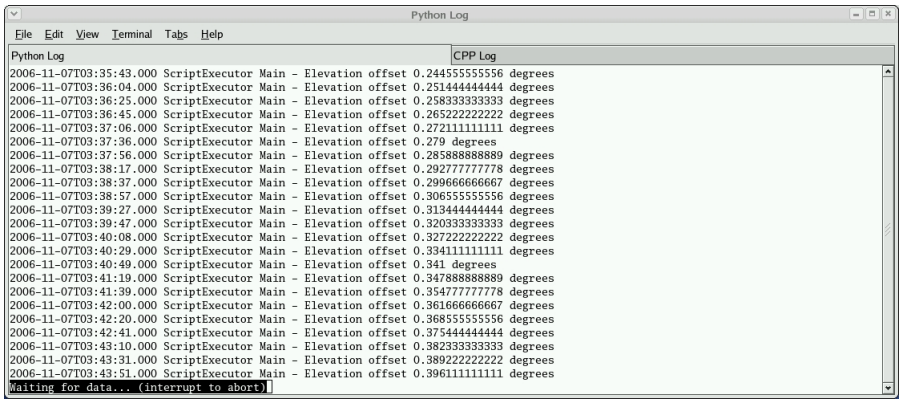

Figure 7: The ATF Log Viewer.

Table 1: Holography Hardware Requirements

Measurement Error	$< 10\mu$m
Phase Accuracy	< 0.3 deg ($2.5\mu m$ @ 3mm) RMS
Amplitude Accuracy	$< 1\%$
Dynamic Range	$\geq$ 43dB
Signal-to-Noise Ratio (SNR)	$\geq$ 40dB
Channel-to-Channel Isolation	$>$ 100dB
Date Rate	$\sim$ 80 samples/second (12 msec sampling)

  - **Select "Acs down" in the OMC GUI:** This stop all of the ACS "containers". Wait for all containers to stop (*i.e.* indicators turn from green to red and show an "error" state.
  - **Select "Session – Exit" from the OMC pull-down menu**
- Shut Down the Antenna if leaving the site: See [Shepherd (2006)] for a description of the antenna START/STOP procedures.

3 Holography System Hardware

The hardware specifications and requirements are summarised in Tables 1 and 2. In the following we briefly describe the hardware components that comprise the holographic measurement system.

3.1 Frontend

The frontend (see Figure 8) is enclosed in a small, temperature controlled box with a diameter of about 30 cm and a length of 50 cm. It fits inside the "apex structure" behind the primary focus of the VertexRSI antenna. The AEC antenna does not provide such a wide space and the receiver is bolted to the outside flange of the apex structure with a long piece of waveguide bringing the signal feed in focus. Both the signal– and reference–receiver are housed "back-to-back" in this box. This provides a compact system in which the LO signals can easily be made equal in length, greatly contributing to the phase stability of the system. Broadband mixers at

Table 2: Holography Hardware Specifications

Frequencies	78.92 and 104.02 GHz
Frequency Stability	$\leq \pm 5$ Hz/day
Receiver Bandwidth	10 kHz
Receiver Tunability	130 MHz
Transmitter Antenna Gain	33dB
Transmitter EIRP	$> 20\mu$W
Transmitter Power to Antenna	> 10nW
Transmitter Antenna Beam Width @ -3dB	4.6 deg (twice antenna angle at xmtr)
Reference Antenna Beam Width @ -3dB	4.6 deg (twice scan range)
Main Feed Beam Width @ -3dB	128 deg (-3dB edge taper)
System Temperature	3200 K
Reference Feed Power Received (P_r)	$1.736 \times 10^{-9} P$
On-Boresight Signal (M_0)	$4.167 \times 10^{-7} P$
On-Boresight Noise (σ_0)	$\left(1.23 \times 10^{-22} W(P)\right)^{\frac{1}{2}}$
Off-Boresight Noise (P_r Term)	$\left(2.13 \times 10^{-27} W(P)\right)^{\frac{1}{2}}$
Average map noise for complex correlator (σ_{av})	$\left(2.23 \times 10^{-25} W(P)\right)^{\frac{1}{2}}$

ambient temperature convert the received signal frequency to a baseband of 10 kHz width. The system is laid out for two frequencies at 78.9 and 104.02 GHz. Making the measurement at two different frequencies can be helpful in discerning systematic effects in the resulting maps, for instance caused by multiple reflections. The receiver is also tunable around each of these frequencies by 130 MHz for similar reasons. The signal horn is a conical, grooved cylindrical waveguide horn, while the reference horn is of similar design and equipped with a lens to provide a reference beam with a beam width of 4.6 degrees at the half-power points.

As is clear from the theoretical treatment given in §6, it is imperative that we know the amplitude and phase function of both the reference and the signal feed as accurately as possible. The phase function must be subtracted from the measured aperture phase before connecting its phase variations to errors in the reflector profile. The feedhorns have been measured with great care on the indoor range at IRAM in Grenoble (IRAM Internal Report, June 2002, by Lazareff, Carter, Halleguen and Degoud). The results were compared with model calculations using an advanced electro-magnetic simulation package and excellent agreement was found. The phase pattern of the feeds have an estimated error of less than one degree, while the amplitude taper at the edge of the reflector aperture is -6 dB. This is more than we would like (a free–space taper of 2.5 dB has to be added to the measured level) for a high signal to noise ratio in the outer part of the reflector; an actual level of -6 dB is preferred. For the measurement of the 64 ALMA production antennas this feed should be replaced by one which provides such a taper.

Figures 9 and 10 show the holography frontend block diagram.

3.2 Backend

The backend of the receiver is essentially a digital signal processor (DSP) where the narrow-band signals are digitized and correlated. Both the “sine” and “cosine” part of the complex correlation function are obtained, which are then transformed to the amplitude and phase functions.

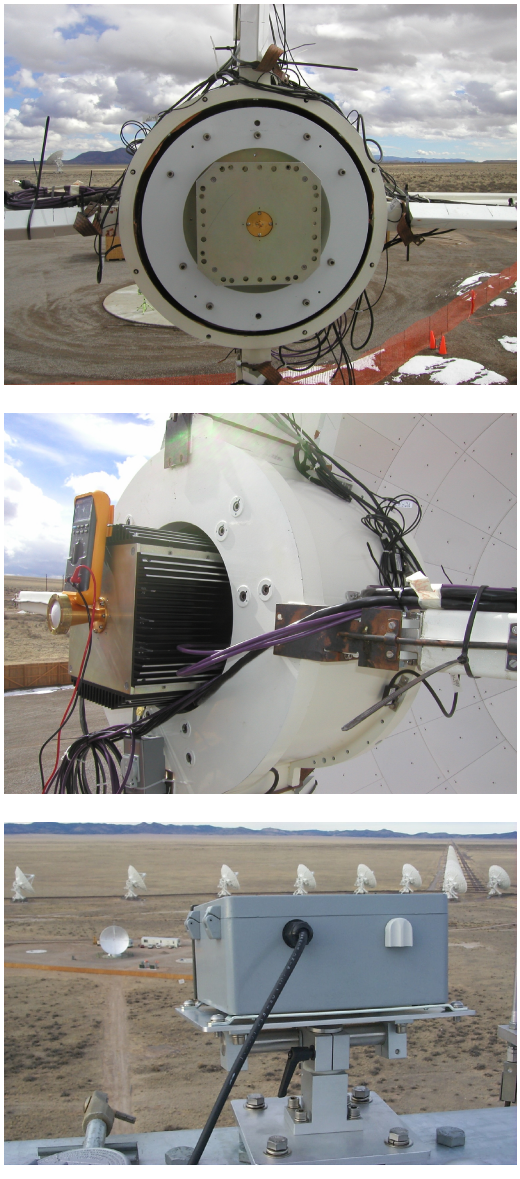

Figure 8: Holography system hardware. Signal feed side of the frontend (top); reference feed side of the frontend (middle); and transmitter (bottom).

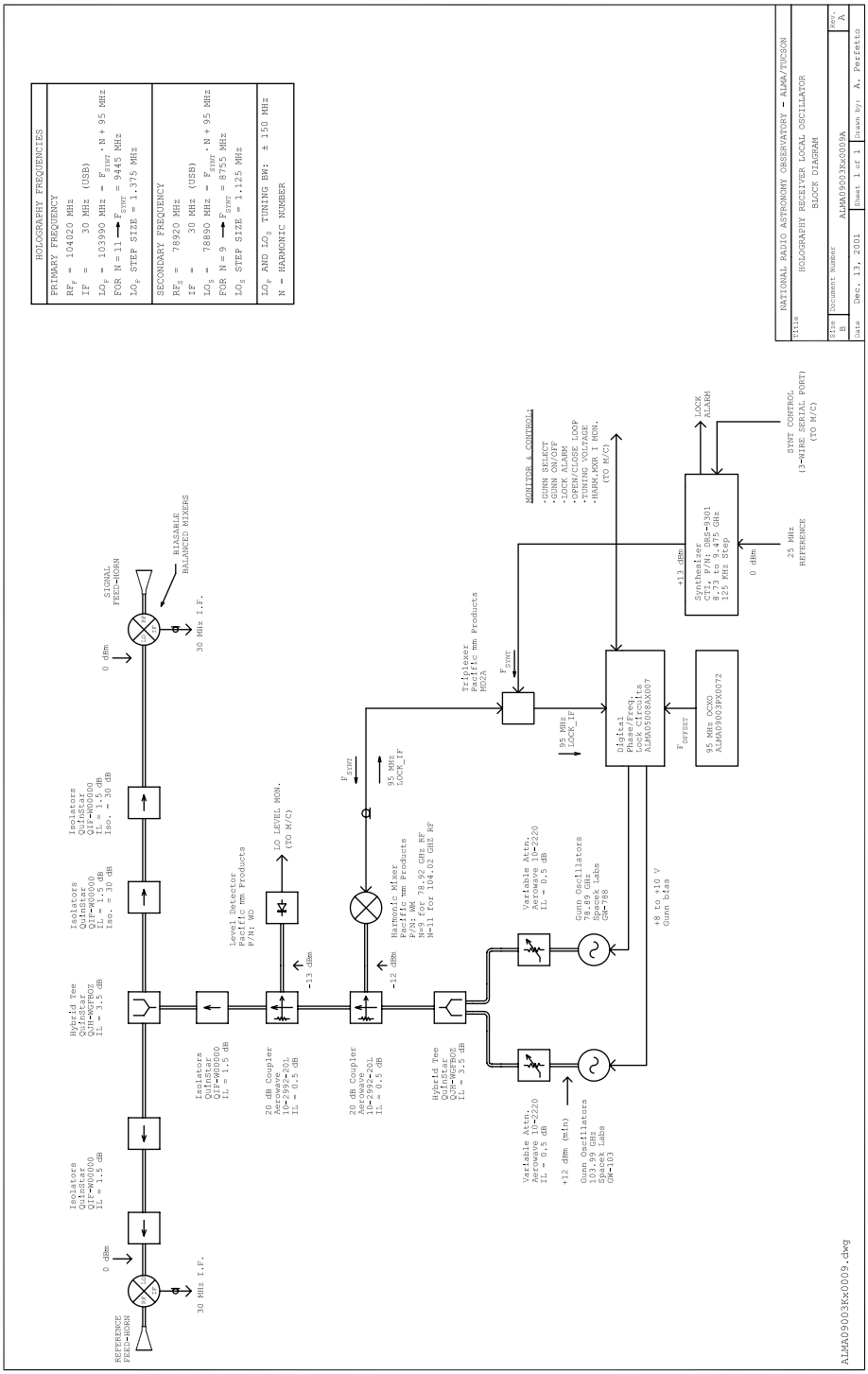

Figure 9: Holography receiver local oscillator block diagram.

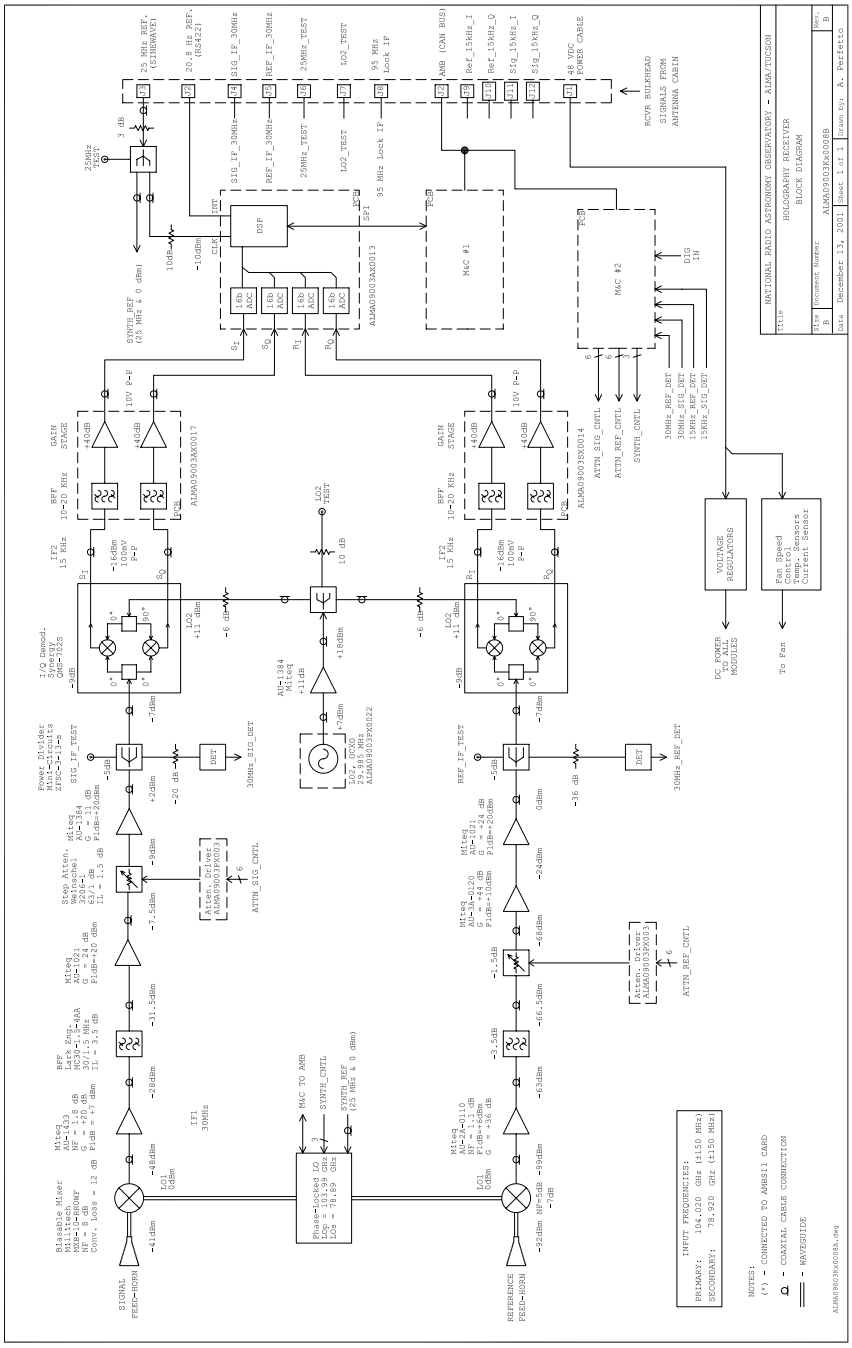

Figure 10: Holography receiver block diagram.

3.2.1 Frontend and Backend Monitor and Control

Monitor and control of the holography frontend is currently done using a LabView interface from a laptop located in the ATF Control Room. Figure 11 shows the two main tabs of this LabView interface. You best become familiar with this interface, as you will find that you will rely on it for most of your monitoring of the health and well-being of the holography receiver. Some things to keep in mind:

- **Signal and Reference Power Setting:** It is best to set the Signal and Reference attenuators such that the total power on boresight is $\lesssim$ 10V. This means that attenuation will be in the following ranges:
  - *Signal: 16 dB (79 GHz) / 0–10 dB (104 GHz).*
  - *Reference: 25 dB (79 GHz) / 6–20 dB (104 GHz).*
- **ACS Monitor and Control:** We have developed a few scripts you can use to tune the holography receiver, dump raw data, etc. See the holography wiki page (reference given in 1) for further information.

3.3 Transmitter

NEED UPDATED DESCRIPTION HERE.

The transmitter consists of a single photo-diode, directly coupled to a waveguide horn, which is fed through an optical fiber by two optical signals at different frequencies near a wavelength of $\sim$ 1550 nm. The photo-diode provides a mixing signal at the difference of the two optical signals, tunable roughly from 78.7 to 79.0 GHz (low band) and 103.8 to 104.2 GHz (high band), with an output power of about 10 nW, leading to an EIRP of about 20 W. The transmitter is placed on top of a 50 m high tower at a distance of 300 to 325 m from the aperture of three antennas at the site, resulting in a measurement elevation angle of about 9 degrees.

Figure 12 shows the holography frontend block diagram.

3.3.1 Transmitter Monitor and Control

A very similar interface as that provided for the holography receiver is used to monitor and control of the holography transmitter. This interface runs on another laptop located in the ATF Control Room. Figure 13 shows this LabView interface. As with the holography receiver GUI, you best become familiar with this interface, as it is the *only* interface to the holography transmitter. Some things to keep in mind:

- **Transmitter Power Setting:** Set the transmitter power to 7 dBm for both bands.
- **Transmitter Frequency Drift:** We have found that the transmitter frequency drifts randomly. You should check whether it is peaked within the 10 kHz band of the receiver by checking it several times a day.
- **Transmitter Power Drift:** We have also found that the transmitter power drifts over 10s of seconds. We have suspects, but no smoking gun for this drift.
- **Information Updates:** See the holography wiki page (reference given in 1) for updated information on this system.

4 Holographic Data Acquisition

To derive typical values for the various holography map parameters, map parameters, we set the following boundary conditions:

1. The data rate is the canonical 12 msec per sample, which means about 80 samples per second.

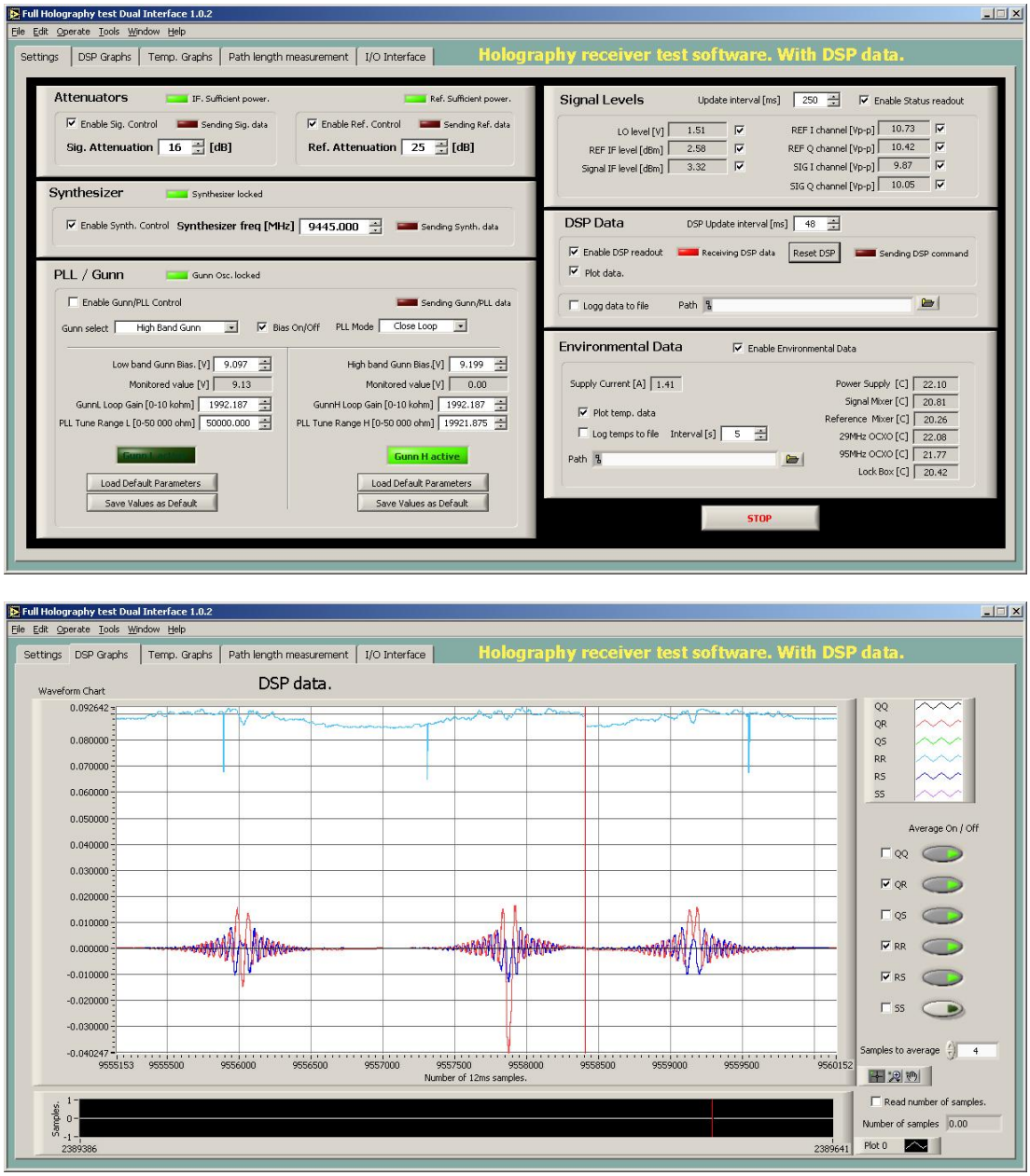

Figure 11: Main control panel (top) and DSP data display (bottom) for the LabView-based holography receiver monitor and control GUI.

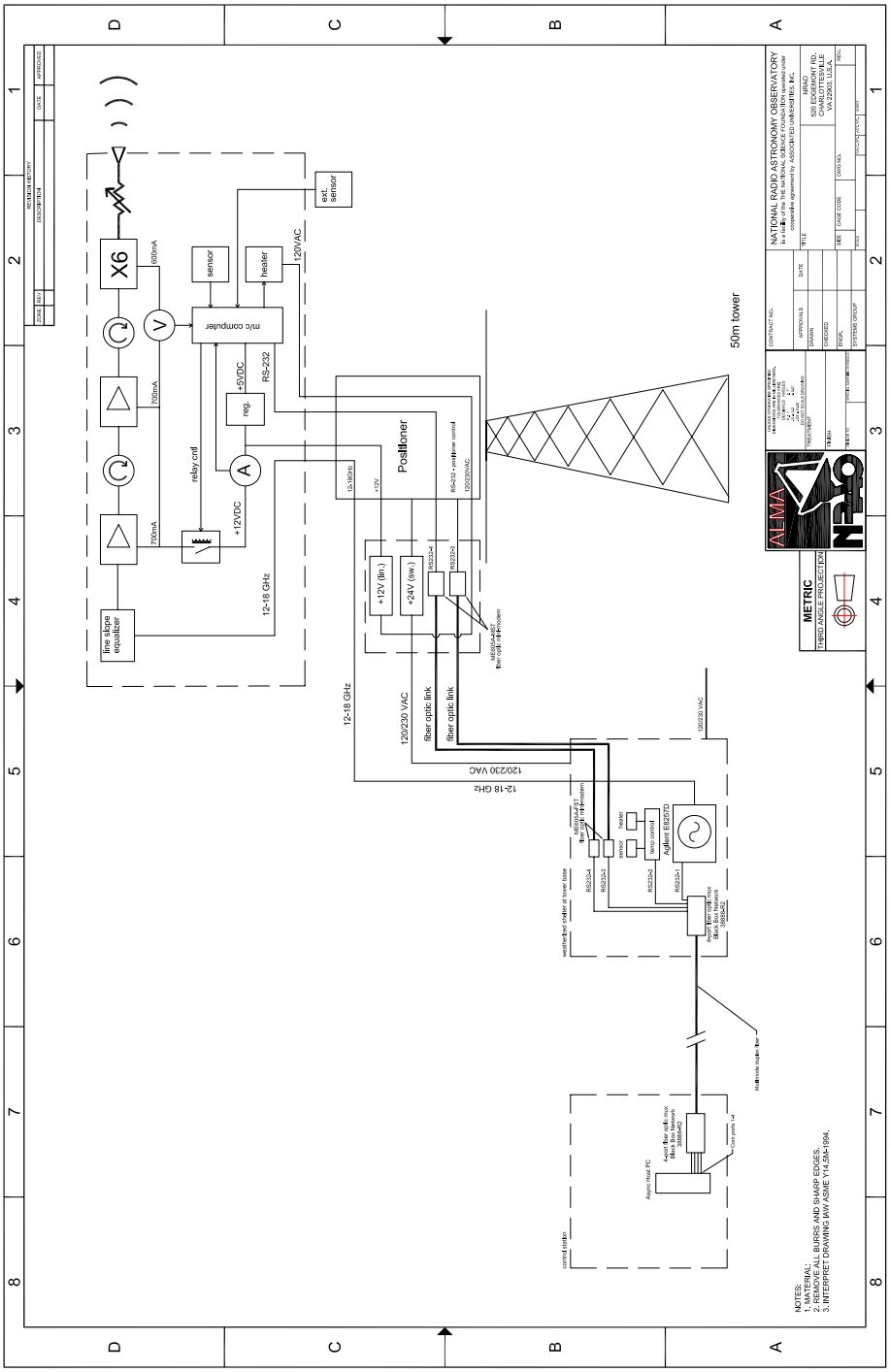

Figure 12: Holography transmitter block diagram.

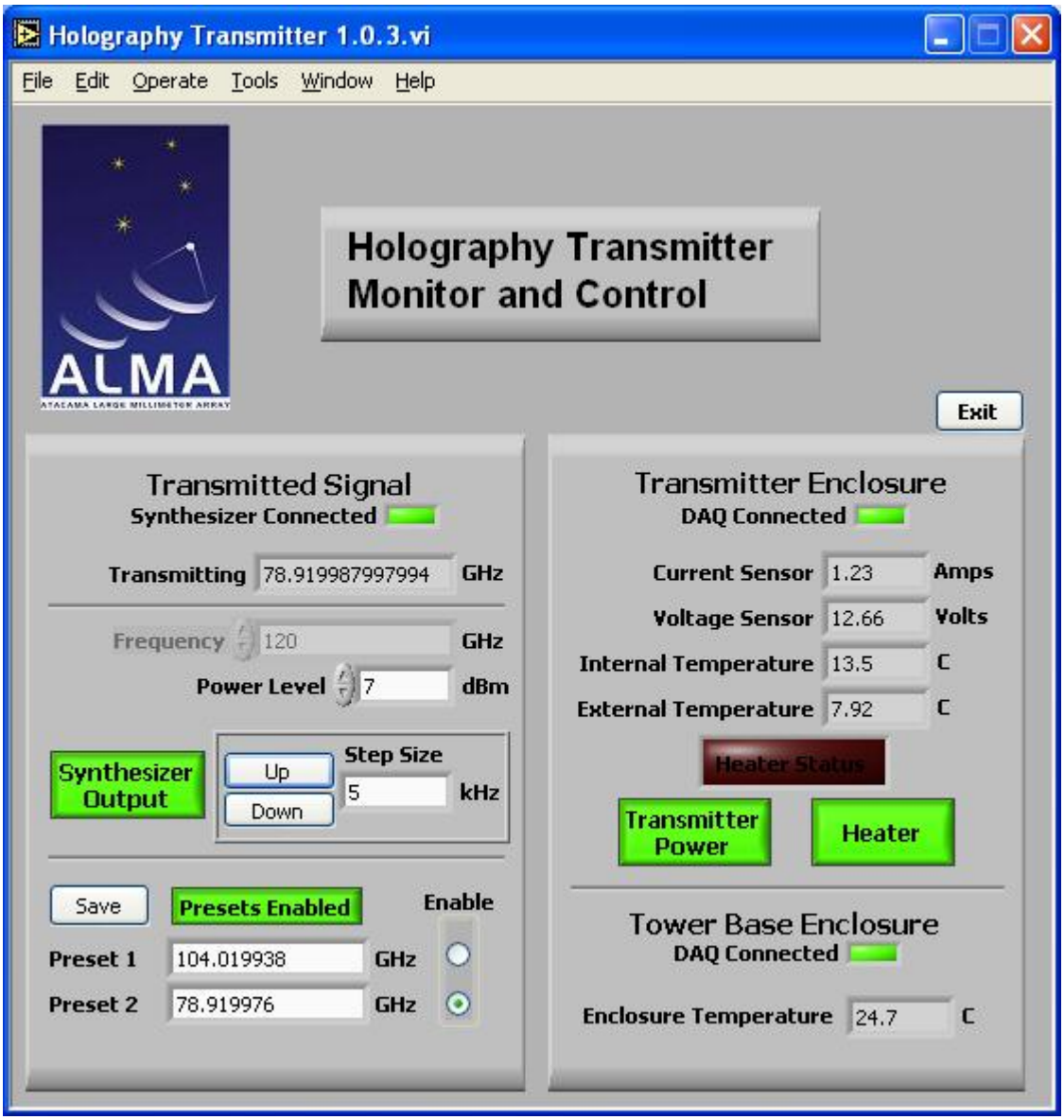

Figure 13: Control panel for the LabView-based holography transmitter monitor and control GUI.

2. The fine tuning feature of the holography receiver allows for the search for ground reflection.
3. A goal for the total time for one map is less than one hour.
4. The required aperture plane resolution is ≤ 20 cm. This yields ≥ 25 independent points per square meter of reflector surface.
5. Oversample by a factor of at least 2 to minimize aliasing.

Based on the equations listed in Appendix A and taking

$$\begin{aligned} f_1 &= 1.13(6 + 2.5 \text{ dB taper}), \\ \nu &= 78.92 \text{ and } 104.02 \text{ GHz}, \\ \theta_b &= 74'' \text{ and } 56'', \end{aligned}$$

we obtain the typical holography map parameters of Table 3.

Table 3: Typical Holography Map Parameters

Map Type	δ_d (cm)	f_{osr}	θ_{ext} (deg)	θ_{sr} ($''$)	$\dot{\theta}$ ($''$/sec)	N_{row}	f_{oss}	t_{map} (hr)
Standard	20	2.2	1.64/1.24	33/25	300	180	20/15	0.96/0.73
Fine	13	2.2	2.46/1.87	33/25	600	270	40/30	1.08/0.82
Less OS	20	1.4	1.64/1.24	53/40	300	112	20/15	0.61/0.46

Assumes constant $f_1 = 1.13$ (6 + 2.5 dB taper).
Assumes $\nu = 78.92/104.02$ GHz and $\theta_b = 74/56$ $''$.
Assumes apodization smoothing factor $f_{apo} = 1.3$.

5 Holographic Data Analysis

THIS SECTION NEEDS TO BE REPLACED WITH UPDATED VERSION.

5.1 Description

Data analysis uses the CLIC data reduction software of the Plateau de Bure interferometer. The raw data, written by the on-line software in the ALMATI-FITS data format [Lucas *et al.* (2001)], is converted to Plateau de Bure format using **CLIC**.

The data are then calibrated and imaged using **CLIC**. The two main operations are:

1. *Calibrate data in amplitude and phase*, based on bore-sight measurements at beginning and end of each map row, assuming gradual drift in amplitude and phase with time. This uses the standard amplitude and phase calibration commands: `SOLVE PHASE, STORE PHASE, SOLVE AMPLITUDE, STORE AMPLITUDE`.
2. *Compute the aperture map and fit panel displacements and deformations*: This is implemented in command `SOLVE HOLOGRAPHY`. The mathematics are in §6.5.

   The data processing steps are:

(a) *Interpolate data to a regular grid* in antenna-based coordinate system. This grid matches the observed system of rows (same number and separation). This grid is further extended, by addition of zeroes, to a user-specified size, in order to get a finer interpolation of the output aperture map: 64x64, 128x128, 256x256 and 512x512 sizes are available.

(b) *FFT to aperture plane.* This is replaced by a more complex transformation if one takes into account the first non-Fresnel terms. This is described in §6.5.

(c) *Compute phases in the aperture plane.*

(d) *Apply the geometrical phase correction*: this is

$$\Delta p = \frac{\rho^2}{2R} - \frac{\rho^4}{8R^3} + \sqrt{\rho^2 + (f + \delta f - \frac{\rho^2}{4f})^2} - (f + \frac{\rho^2}{4f} + \delta f)$$

where ρ is the radius in the aperture, f the focal length of the primary, δf the refocusing used to compensate for the finite transmitter distance R (δf is the distance between the holographic horn phase center and the antenna prime focus). See §6.5.

(e) *Correct for measured feed phase diagram.*
The measurement is described in the memo by [Lazareff *et al.* (2003)].

(f) *Mask edges and blockage.*

(g) *Fit and remove 6 phase terms:* constant, 2 linear gradients, 3 focus translations. They account for a phase offset, an antenna pointing error (constant during the measurement) and a small displacement of the holography horn relative to the nominal focus position ($f + \delta f$ above). One may keep fixed either the X and Y coordinates or all three X, Y, Z coordinates.

(h) *Convert to normal displacement map.*

(i) *Plot amplitude and phase maps.*

(j) *Fit panel displacements (optionally deformations) and screw adjustments.*
In CLIC we deconvolve for finite resolution effects by an iterative procedure (subtracting the truncated field of the fitted panels from the measurements, to get the next order correction, ...). The screw settings are output in a text file (*e.g.* `23-jul-1996-Vertex.panels`).

We introduced also a correction to add empirically an offset to the central pixel of the beam map, in order to partially cancel the ring pattern. The best offset was selected on the basis of the improvement on the final surface rms. This did not prove very successful in removing the ringing pattern.

5.2 Using the GUI Interface

— Type `clic` in a terminal window.

— Type `@ ATFdefine`. A small menu window should appear on the screen.

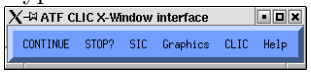

— In menu `CLIC`, select `ATF Holography reduction`. This causes a graphic window to appear, as well as a dialogue window.

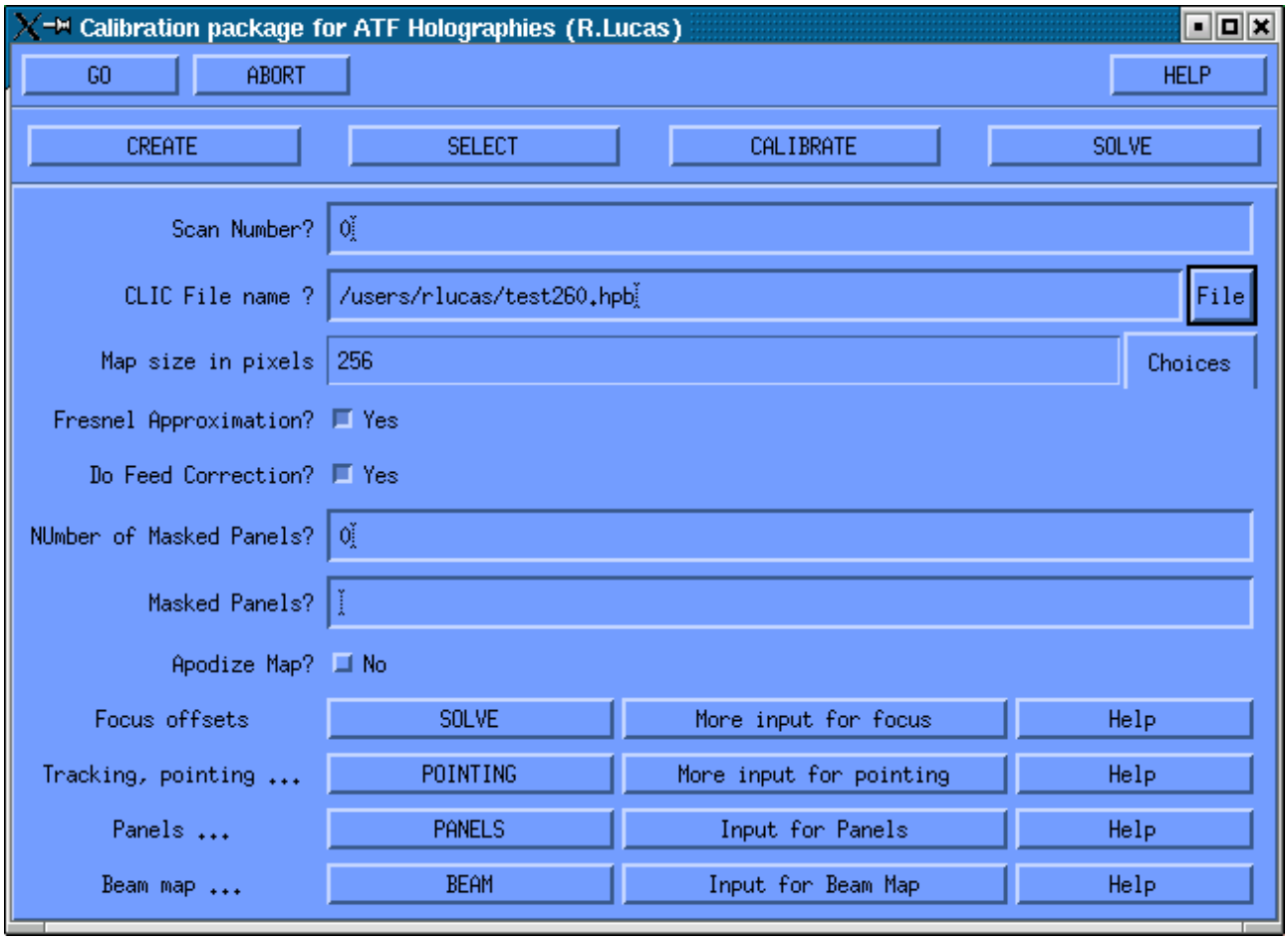

— Enter the scan number (there is one FITS file per scan; they reside in `/users/oper/HOLODATA/` under the names `TESTnnnn.FITS`, where `nnnn` is the scan number).
— Press "`CREATE`". This will copy the FITS data into a CLIC data file. Its name will be `testnnnn.hpb`.
— Press "`SELECT`". You should get a plot of angular offsets versus scan number.
— Press "`CALIBRATE`". Amplitude and phase of the boresight measurements will be displayed together with a red curve fit. Enter `continue` or press `CONTINUE` at the left of the ATF menu window, if the fit looks all right, in order to store it within the data headers.

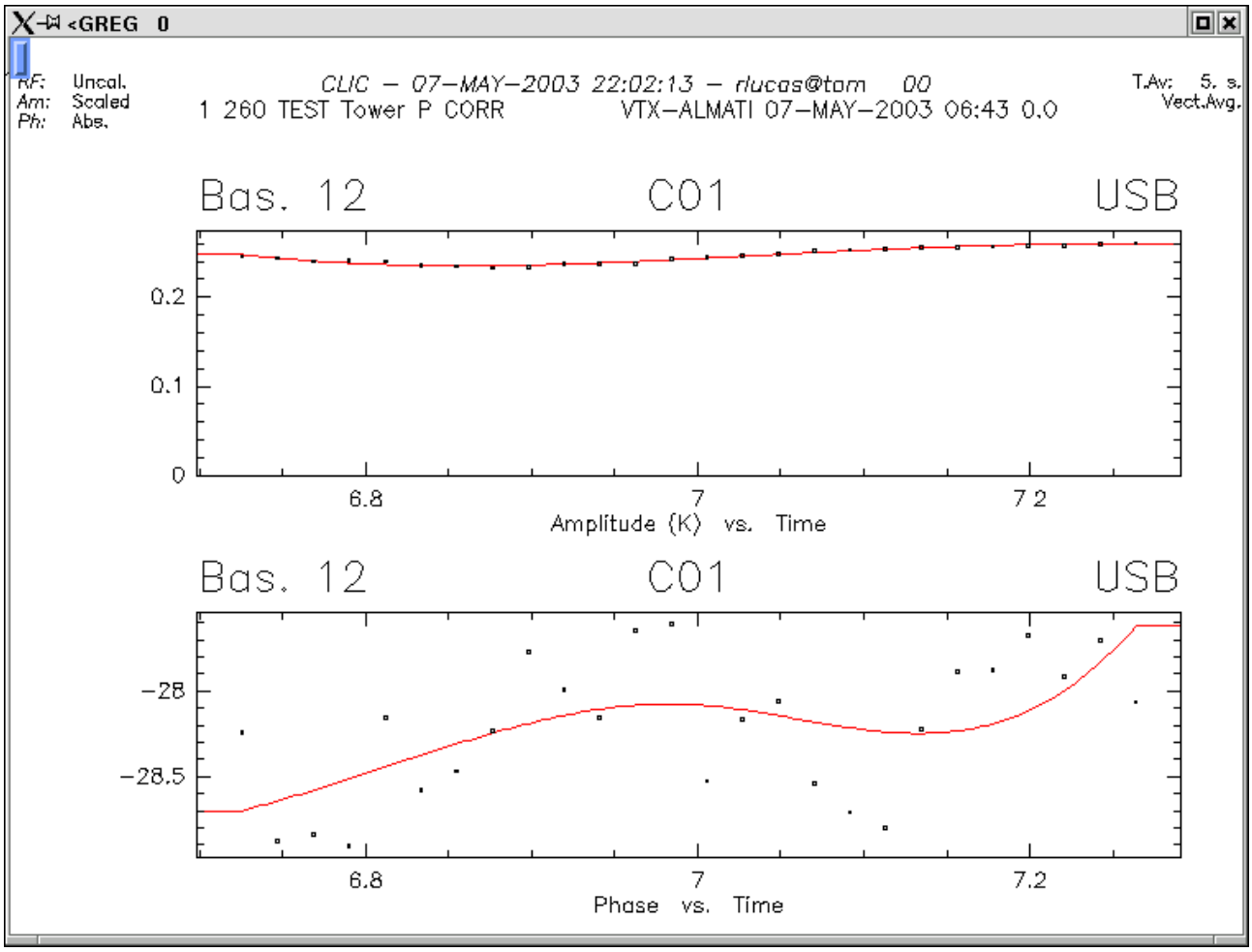

It the fit fails, e.g. due to fast variations, or bad points :

- You may change the step of the spline fuction (`SET STEP value`, with value in hours), then `SOLVE AMPLITUDE PHASE /PLOT`, to get a new fit.
- Or you may delete a bad point by finding its observation number:
  - enter `CURSOR`, point with the mouse to the bad point and type '`H`'. The first number listed will be the observation number `n` .
  - Then type `DROP n` to eliminate this observation from the current index.
  - Then type `SOLVE AMPLITUDE PHASE /PLOT`, to get a new fit.
- When you are satisfied, do not forget to type `C` (for `CONTINUE`), so that the calibration is stored within the data headers.

- Select the map size in pixels (64 to 512). It should be higher than the actual number of rows in the observed beam map, (or information will be lost).
- Press "`SOLVE`". The map should appear in the graphic window.

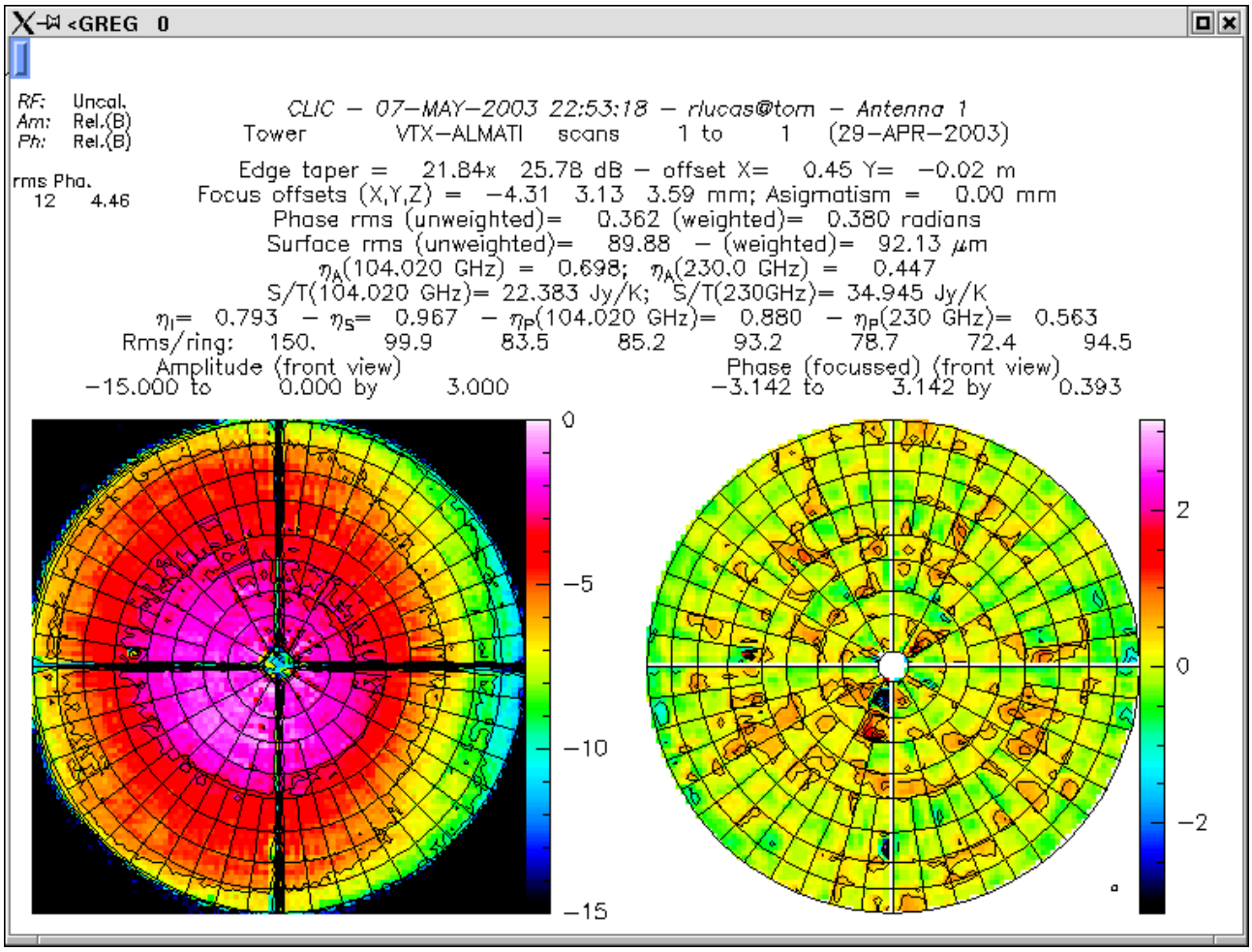

The map header contains, among other parameters:

- — the illumination parameters,
- — the phase rms (unweighted and weighted by the amplitude),
- — the surface rms (also weighted and unweighted),
- — aperture efficiencies (calculated using the observed illumination and the geometrical blockage, for the observed frequency and 230GHz), and the corresponding Jy to Kelvin conversion factors,
- — illumination efficiency, spillover efficiency, and phase efficiencies (Ruze factors)
- — the surface rms in each ring.

— Additional parameters in the main window:

- — *Fresnel Approximation*: when selected, the additional terms (see §6.2.
- — *Do feed Correction*: to be unselected for testing only.
- — *Number of masked panels*: the number of panels to be ignored for the fit and the calculation of RMS surface errors. Their numbers are entered in the box below. The panel numbering scheme is in Appendix B.

  - *Apodize Map*: to apodize the observed map in order to reduce/suppress the 'ringing' along the quadrupod legs and map edges. The weighting function is a cosine reaching zero at the map edges.
- Additional input windows (to call them press on e.g. "`More input for focus`", and the similar boxes below):
  - `Focus offsets`: Enter here the focus offsets in mm. The corresponding corrections are applied to the phase map before fitting for focus displacements. This enables overcoming the 2π discontinuities in the phase map. One may also fix either the X and Y focus coordinates, or all X, Y and Z to these values.

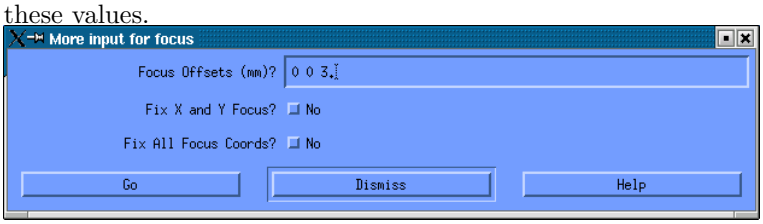

  - `Tracking, Pointing` : The input map can be displaced to compensate for pointing errors, if they are larger than a fraction of a beam. Naturally it is preferred to peak up on the transmitter before taking the map. One may also enter a 'fudge factor' to correct for a tracking error which changes sign between odd and even rows of the map.

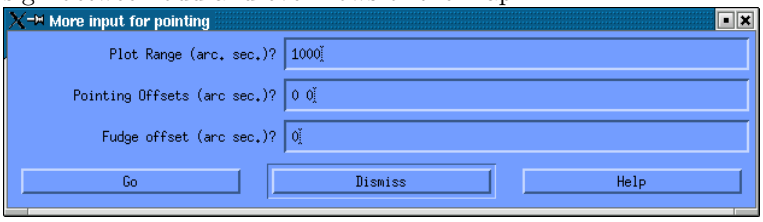

  - The last row is used to `plot a beam map`.

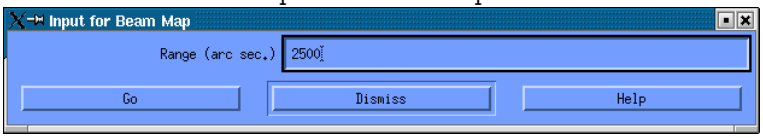

- To obtain the list of screw settings: Press "`PANELS`". A file such as `23-nov-2001-Vertex.panels` is created (where positive numbers mean that the panels should move towards the subreflector). It contains the screw motions in micrometers. At the end of the calculation the left part of the screen displays the fitted panel shapes, while the right one displays the fit residuals.
- Specific options for this last step can be seen and entered by pressing "`input for panels`". Additional input include:
  - *Modes:* the fitted degrees of freedom for panel fitting; the last two actually deform the panels:

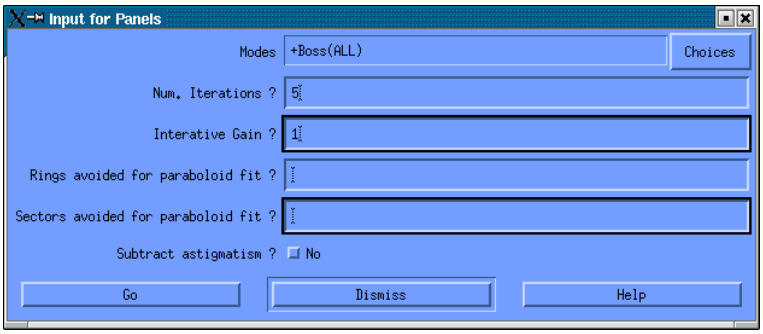

Piston only 1 translation mode (normal to antenna surface)

+Tilts 3 modes: panel tilts around two perpendicular axes in the tangent plane to the paraboloid are added

+Torsion 4 modes: a panel torsion is added

+Boss 5 modes: the motion of panel center relative to the edges is added.

— *Number of iterations:* usually 5 is OK

— *Iterative gain:* usually 1 works

— *Rings avoided for paraboloid fit:* One may take out specific rings of the paraboloid fit (e.g. to adjust one or several ring relative to the others).

— *Sectors avoided for paraboloid fit:* One may take out specific sectors of the paraboloid fit (e.g. to adjust one sector relative to the others).

— *Substract astigmatism:* Take out the astigmatism component before fitting the panels.

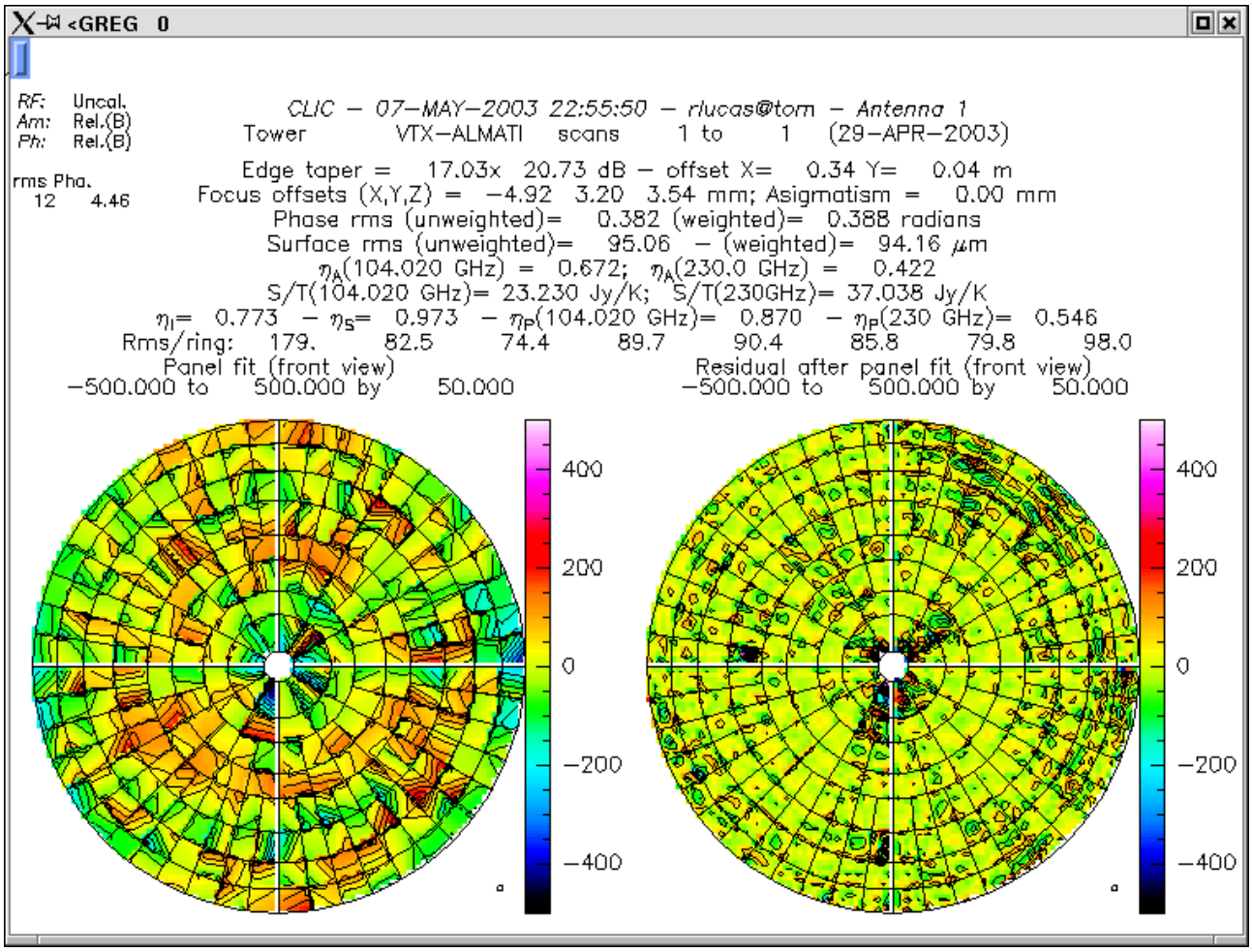

— Sample screw listing (Positive screw settings mean that the panel has to move closer to the primary focus, or "up"):

```
 Output from CLIC\SOLVE HOLO            3
 CLIC - 07-MAY-2003 22:55:50 - rlucas@tom - Antenna 1
 Tower        VTX-ALMATI   scans     1 to     1   (29-APR-2003)

Panel ring n0.  1:
 Sec/Pan     Screw settings (1-5), [mum]
    1-11       -192( 37)  -216( 37)   -36( 59)  -117( 59)  -117( 28)
    2-11        -36( 41)   105( 41)  -167( 64)   319( 64)   -11( 31)
    3-11       -230( 30)  -174( 30)   -79( 48)   115( 47)  -100( 22)
    4-11        -97( 28)  -107( 28)   -42( 44)   -78( 44)   -72( 21)
    5-11        -82( 29)  -127( 29)    -3( 44)  -156( 44)   -68( 21)
    6-11       -174( 33)  -165( 33)    30( 52)    59( 52)   -47( 25)
    7-11       -159( 15)  -229( 15)   127( 23)  -116( 23)   -41( 11)
```

```
    8-11        -38( 22)   -32( 22)    77( 34)    97( 34)    34( 16)
    9-11       -499( 61)  -469( 61)  -197( 96)   -92( 96)  -298( 46)
   10-11        -39( 49)   -16( 49)   -59( 79)    20( 78)   -34( 37)
   11-11          5( 29)   -81( 29)   115( 45)  -181( 45)     8( 21)
   12-11       -161( 23)  -267( 23)   113( 37)  -251( 37)   -76( 18)

Panel ring n0.  2:
 Sec/Pan     Screw settings (1-5), [mum]
    1-21          9( 19)    86( 19)  -100( 19)     7( 19)   -11(  9)
    2-21        -67( 32)    18( 32)  -182( 31)   -65( 31)   -87( 16)
    3-21         -2( 12)   -70( 12)   -21( 12)  -115( 12)   -44(  6)
    4-21        -20( 23)   -11( 23)   -48( 23)   -35( 23)   -30( 11)
    5-21        -30( 18)   -77( 18)    52( 17)   -13( 17)   -10(  9)
    6-21         -3(  9)   -35(  9)    66(  9)    21(  9)    18(  4)
    7-21         59( 18)   -31( 18)    80( 18)   -44( 18)    27(  9)
    8-21        -30( 13)    50( 13)   -45( 13)    66( 13)     0(  7)
    9-21         57( 38)    58( 38)   175( 39)   176( 38)   119( 19)
   10-21        -39( 15)   -19( 15)    27( 15)    55( 15)     5(  8)
   11-21        -42( 11)  -101( 11)     0( 11)   -82( 11)   -48(  6)
   12-21        -60( 13)   -72( 13)   -16( 13)   -32( 13)   -43(  6)

Panel ring n0.  3:
 Sec/Pan     Screw settings (1-5), [mum]
    1-31        -33( 13)   -13( 13)    13( 14)    44( 13)     4(  6)
    1-32         35( 13)    -6( 13)    98( 14)    37( 14)    43(  6)
    2-31         30( 11)   -42( 11)    41( 11)   -65( 11)    -9(  5)
    2-32       -130( 24)  -100( 24)    81( 26)   125( 25)     0( 10)
    3-31        -90( 12)   -19( 12)   104( 12)   209( 12)    57(  5)
    3-32        -66( 20)  -126( 20)   192( 22)   103( 21)    33(  9)
    4-31        113( 13)   -34( 13)   108( 14)  -110( 14)    18(  6)
    4-32         90( 19)   111( 19)    12( 20)    43( 19)    62(  8)
    5-31       -121( 27)  -152( 27)    26( 29)   -21( 29)   -63( 12)
    5-32         26( 23)    46( 23)   -84( 24)   -55( 24)   -20( 11)
    6-31        141( 16)    72( 16)   154( 16)    52( 16)   104(  7)
    6-32         24( 16)    45( 16)    -5( 17)    25( 17)    22(  7)
    7-31        -47( 11)  -110( 11)    -9( 12)  -101( 12)   -66(  5)
    7-32         12( 14)    -2( 14)   126( 15)   105( 15)    63(  6)
    8-31         89( 11)    58( 11)    98( 11)    52( 11)    74(  5)
    8-32         13(  6)     7(  6)    50(  7)    41(  7)    29(  3)
    9-31         31( 20)    16( 20)    68( 21)    47( 21)    42(  9)
    9-32        -49( 22)   -38( 22)   -70( 24)   -54( 23)   -53( 10)
   10-31       -120( 20)   -48( 20)     1( 21)   107( 21)   -11(  9)
   10-32         26( 14)     7( 14)    72( 15)    44( 15)    38(  6)
   11-31         21( 10)     9( 10)   154( 10)   136( 10)    84(  5)
   11-32        -40( 16)   -41( 16)    30( 17)    29( 17)    -3(  7)
   12-31         38(  8)    24(  8)    23(  8)     3(  8)    21(  4)
   12-32       -126( 19)   -40( 19)   -53( 20)    73( 20)   -34(  9)

Panel ring n0.  4:
```

Sec/Pan	Screw settings (1-5), [mum]				
1-41	86(11)	10(11)	152(11)	58(11)	70(5)
1-42	33(12)	7(12)	16(13)	-16(12)	12(6)
2-41	-21(15)	-76(15)	12(16)	-56(16)	-38(8)
2-42	113(14)	48(14)	114(15)	34(15)	78(7)
3-41	156(9)	135(9)	111(9)	85(9)	127(4)
3-42	34(18)	121(18)	41(19)	148(18)	84(9)
4-41	114(29)	142(29)	81(30)	115(30)	116(14)
4-42	7(20)	55(20)	-13(21)	47(21)	25(10)
5-41	-35(21)	89(21)	-29(22)	124(22)	35(10)
5-42	94(10)	88(10)	77(10)	70(10)	84(5)
6-41	73(17)	109(17)	-58(18)	-13(18)	41(9)
6-42	83(14)	16(14)	105(15)	23(14)	55(7)
7-41	-23(19)	-2(19)	-36(20)	-9(20)	-17(9)

... and so on until:

12-84	-231(46)	-31(45)	-262(47)	-41(46)	-141(21)

The adjustments were done with a simple tool. Two people on a man-lift approached the surface from the front, where the adjustment screws are located (see Figure 14). The time needed for an adjustment of the total of 1320 adjusters was 8 hours. The specification requires a full adjustment in 8 hours. In the series production, with the use of a more automated tool, this should be readily achievable.

6 The Holographic Method

This section excerpted from "Near-Field Radio Holography of Large Reflector Antennas" by J. W. M. Baars, R. Lucas, J. G. Mangum, and J. A. Lopez-Perez, IEEE Antennas and Propagation Magazine, 2006 (in press).

We summarise the mathematical foundation of the holographic method of measuring the reflector profile of an antenna or radio telescope. In particular, we treat the case, where the signal source is located at a finite distance of the antenna under test, necessitating the inclusion of the so-called Fresnel field terms in the radiation integrals. We assume a "full phase" system with reference receiver to provide the reference phase. Thus so-called phase-recovery schemes are not discussed here. These have been extensively described by [Morris (1985)].

Large reflector antennas, as those used in radio astronomy and deep-space communication, generally are composed of a set of surface panels, supported on three or more points by a support structure, often called the backup structure. After assembly of the reflector it is necessary to accurately locate the panels onto the prescribed paraboloidal surface in order to obtain the maximum antenna gain. The fact that some antennas have a "shaped"contour is irrelevant for the purpose of our discussion. We are concerned with describing a method which allows us to derive the position of the individual panels in space and compute the necessary adjustments of their support points to obtain a continuous surface of a certain prescribed shape.

The analysis by [Ruze (1966)] of the influence of random errors in the reflector contour on the antenna gain indicates that the rms error should be less than about one-sixteenth of the wavelength for acceptable performance. Under the assumption that the errors are randomly distributed with rms value ϵ and have a correlation length $\mathbf{c}$ which is much larger than the wavelength λ and much smaller than the reflector diameter D, the relative decrease in aperture efficiency (or gain) can be expressed by the simple formula

Figure 14: Panel adjustment of the VertexRSI prototype antenna.

$$\frac{\eta_A}{\eta_{A0}} = \exp\left\{-\left(\frac{4\pi\epsilon}{\lambda}\right)^2\right\}, \tag{1}$$

where η_{A0} is the aperture efficiency of the perfect reflector. Note that:

— The above is true only if $\epsilon \lesssim \frac{\lambda}{8}$.

— An error of $\lambda/40$ is required to limit the gain loss to 10 percent.

The first large reflectors for radio astronomy, here also called radio telescope, had a diameter of about 25 m and operated at wavelengths longer than 10 cm. Thus a surface precision of several millimeters would have provided excellent performance. A measurement accuracy of this order-of-magnitude is readily achievable with a classic "theodolite and tape" method. Using the best theodolites (T3), accuracies of the order of 100 micrometers have been achieved on reflectors of a size up to 30 m [Greve (1986)]. However, the development of the technology of large and simultaneously highly accurate antennas has been a very active field over the last 30 years, whereby the application of the design principle of homology [von Hoerner (1967)] has enabled the construction of, for instance, a 100 m diameter radio telescope with a surface accuracy of about 0.5 mm [Hachenberg *et al.* (1973), Godwin *et al.* (1986)], a 30 m millimeter telescope with 75 μm accuracy [Baars *et al.* (1987), Baars *et al.* (1994)] and 10-12 m diameter submillimeter telescopes with an rms surface error of less than 20 μm ([Baars *et al.* (1999)]). The setting of the reflector panels at such high accuracy has required the development of measuring methods of hitherto unsurpassed accuracy. It should be noted that these measurements need to be done "in the field", which in the case of millimeter radio telescopes often means the hostile environment of a high mountain site.

A number of special measuring methods and devices have been developed (for a review, see [Baars (1983)]). The most versatile, and by now widely used method is normally called "radio holography". The method makes use of a well-known relationship in antenna theory: the far-field radiation pattern of a reflector antenna is the Fourier Transformation of the field distribution in the aperture of the antenna. Note that this relationship applies to the amplitude and phase distributions, not to the power pattern. Thus, if we can measure the radiation pattern, *in amplitude and phase*, over a sufficiently large angular area, we can derive by Fourier Transformation the amplitude and phase distribution in the antenna aperture plane with an acceptable spatial resolution. The latter is determined by the angular size of the measured radiation pattern. This method was suggested, but not worked out in any detail, in the appendix of Jennison's pocket book "Radio Astronomy" [Jennison (1966)]. The paper by [Bennett *et al.* (1976)] presented a sufficiently detailed analysis to draw the attention of radio astronomers. Thus, [Scott & Ryle (1977)] used the new Cambridge 5 km array to measure the shape of four of the eight antennas, using a celestial radio point source and the remaining antennas to provide the reference signal.

The use of a natural, celestial signal source is very attractive for two reasons. First the source is definitely in the far-field of the antenna. The **far-field region** of the antenna is defined to start at

$$R_f = \frac{2D^2}{\lambda}, \tag{2}$$

and can easily reach values of several hundreds of kilometers. Thus no earth-bound transmitter will ever be in the far-field for these applications. Secondly, the celestial radio source traces a daily path across the sky, providing a range of elevation angles over which the data can be collected. This is of great interest for the study of elevation dependent deformations of the antenna, caused by gravity. However, normally the intensity of the cosmic source is not sufficient to achieve the required signal-to-noise ratio for an accurate measurement. Only

a few strong sources are available. The situation is more favourable if there are several large antennas, as in interferometric arrays, where the extra antennas can be used to provide a strong reference signal.

For the IRAM 30 m millimeter telescope on Pico Veleta [Baars *et al.* (1987)] it was decided to use a holographic system at 22 GHz, using the giant water vapour maser in the Orion Nebula, which flared to an intensity of several million jansky during the design phase of the telescope. The reference signal was provided by a 1.5m diameter reflector located in the back of the prime-focus cage of the telescope. A compact double receiver in the prime focus served both reference and main reflector. Although by the time of the measurement the maser source had weakened, it was sufficiently strong to enable a measurement of the surface with an accuracy of about 30 μm rms and a setting of the surface to better than 100 μm rms [Morris (1988)].

Artificial satellites, radiating a beacon signal at a fixed frequency can also be used as far-field signal source. Extensive use has been made of synchronous communication satellites in the 11 GHz band (*c.f.*[Godwin *et al.* (1986)]. These transmitters of course do not provide the range of elevation angles accessible with cosmic sources. Some satellites, notably the LES (Lincoln Experimental Satellite) 8 and 9, have been used for radio holography of millimeter telescopes (*c.f.*[Baars *et al.* (1999)]. They provided a signal at the high frequency of 37 GHz and with their geo-synchronous orbit moved over some 60 degrees in elevation angle. Unfortunately, both satellites are no longer available. Radio astronomers would be greatly helped if a satellite would become available with a reliable transmitter at a high frequency of about 40, or preferably 95 GHz.

Lacking a sufficiently strong source in the far-field, we have to take recourse to using an earth-bound transmitter. In practice these will be located at a distance of several hundreds of meters to a few kilometers and be at an elevation angle of less than 10 degrees. Clearly, these are in the near-field of the antenna, requiring significant corrections to the received signals. The detailed treatment of this case is presented in this report.

Successful measurements on short ranges have been reported for the JCMT [Hills *et al.* (2002)] and the ASTE antenna of NAOJ. The ALMA prototype antennas (12 m diameter, surface accuracy 20-25μm) have been measured and set with the aid of a transmitter at a distance of 315 m, elevation angle 9 degrees, radiating at a wavelength near 3 mm. We will discuss the results of these measurements in this report.

6.1 The Mathematics of Radio Holography

The reciprocity theorem describes the equivalency between the characteristics of a transmitting and receiving antenna. Thus both concepts will be used in the following treatment depending on the specific aspect under description. We shall not repeat here the fundamental analysis which leads from Maxwell's equations to the "physical optics" representation of the characteristics of the reflector antenna (see *e.g.* [Silver (1949)] and [Rusch & Potter (1970)]). The basic expression, linking the radiation function $f(x, y, z)$ at a point P in space with the field distribution $F(\xi, \eta)$ over the aperture plane of the antenna, is written as (see Figure 15 for the geometry)

$$f(x,y,z) = \frac{1}{4\pi} \int F(\xi,\eta) \frac{e^{-ikr}}{r} \left[\left(ik + \frac{1}{r} \right) \boldsymbol{i_z} \cdot \boldsymbol{r_1} + ik \boldsymbol{i_z} \cdot \boldsymbol{s} \right] d\xi d\eta, \tag{3}$$

where the integration is extended over the aperture area, $k = 2\pi/\lambda$ and the unit vectors are as indicated in Figure 15 (with $\mathbf{s}$ the propagation vector of the wave field in the aperture). This relation assumes that the aperture is large in units of the wavelength. This general expression can be simplified depending on the distance of the field point P from the aperture plane. We discern the so-called far-field region (Fraunhofer diffraction), nearfield region (Fresnel diffraction) and the evanescent wave zone up to a few wavelengths from the reflector. In the last case, which does not concern us here, no approximations are allowed.

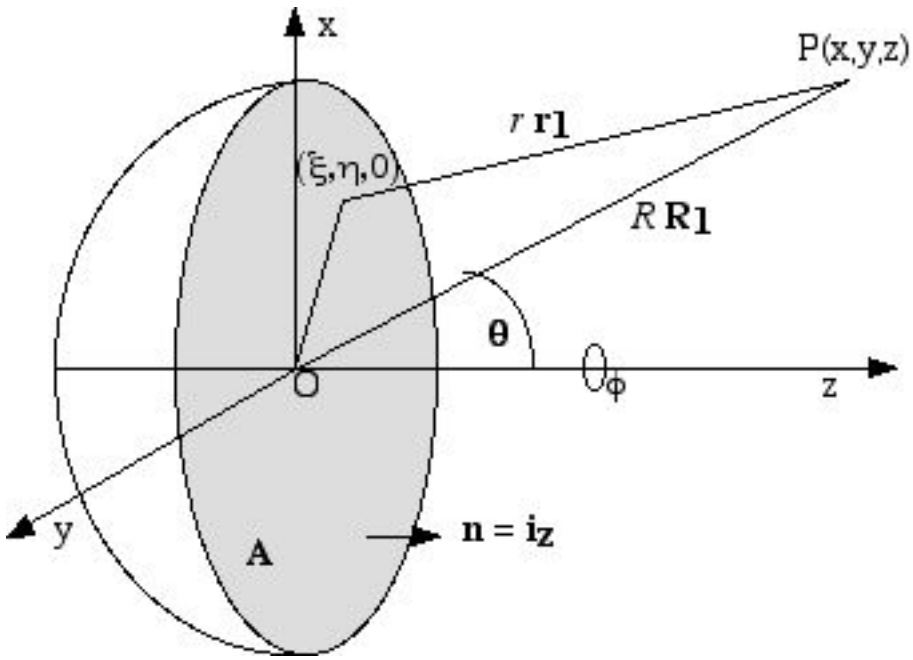

Figure 15: Geometry of the aperture integration method for finite distance to the field point P.

6.2 The Nearfield Approximation (Fresnel Region)

In the **nearfield** region, which corresponds to the Fresnel region in optical diffraction (*c.f.*[Born & Wolf (1970)]) some simplifications can be introduced in the evaluation of Equation 3:

1. r is large enough to ignore its inverse with respect to k in the bracketed term
2. the term 1/r outside the brackets is replaced by the reciprocal distance 1/R from the aperture center to the field point P.
3. the term $\boldsymbol{i_z} \cdot \boldsymbol{r_1}$ can be approximated by $\boldsymbol{i_z} \cdot \boldsymbol{R_1} = \cos\theta$ with R_1 the unit vector from the origin to the field point.
4. the term $\boldsymbol{i_z} \cdot \boldsymbol{s}$ represents a deviation from uniform phase over the aperture. If these are small, this term can be assumed to be equal to one over the aperture.

Note that the variation in r over the aperture must be maintained in the exponent (phase) term. This gives rise to the well-known Fresnel integrals.Thus the nearfield (Fresnel region) expression can be written as

$$f(x,y,z) = \frac{i}{2\lambda R} \int F(\xi,\eta)\,[\cos\theta + 1]\, e^{ikr} d\xi d\eta. \tag{4}$$

We have (see Figure 15)

$$r = \left\{ (x-\xi)^2 + (y-\eta)^2 + z^2 \right\}^{0.5}. \tag{5}$$

Writing the coordinates of the field point P(x,y,z) in spherical coordinates, we obtain

$$\begin{aligned} x &= R\sin\theta\cos\phi \equiv Ru, \\ y &= R\sin\theta\sin\phi \equiv Rv, \\ z &= R\cos\theta = R\sqrt{(1-u^2-v^2)}, \end{aligned}$$

where we have also introduced the **direction cosines** of the field point

$$P(u, v = \sin\theta\cos\phi, \sin\theta, \sin\phi). \tag{6}$$

Thus, Equation 5 can be written as

$$\begin{aligned} r &= \{(Ru-\xi)^2 + (Rv-\eta)^2 + R^2(1-u^2-v^2)\}^{0.5} &(7)\\ &= R\left\{1 - 2\frac{u\xi+v\eta}{R} + \frac{\xi^2+\eta^2}{R^2}\right\}^{0.5}. &(8) \end{aligned}$$

The series expansion of Equation 8 yields

$$r \approx R - (u\xi+v\eta) + \frac{\xi^2+\eta^2}{2R} - \frac{(\xi^2+\eta^2)^2}{8R^3} - \frac{(u\xi+v\eta)^2}{2R} + \frac{(\xi^2+\eta^2)(u\xi+v\eta)}{2R^2} - \ldots \tag{9}$$

Normally, for the Fresnel region analysis, the series is stopped after the quadratic term, which preserves the first three terms of the series in Equation 9. This leads from Equation 4 to the following radiation integral

$$f(u,v) = \frac{i}{\lambda}\frac{e^{ikR}}{R}\int F(\xi,\eta)\exp\left\{ik\left[-(u\xi+v\eta) + \frac{\xi^2+\eta^2}{2R}\right]\right\}d\xi d\eta. \tag{10}$$

The integral of Equation 10 is the well known Fresnel diffraction integral in two coordinates.
Considering that for a high gain antenna, the angular region of interest is confined to small values of θ, we can write in Equation 4 $\cos\theta = 1$, which is valid to 0.1 % for angles up to 3 degrees off axis. If we introduce into Equation 10 the spherical coordinates, defined above, and define the aperture as a circular plane with radius **a**, radial coordinate ρ and azimuthal angle χ, the integral takes the form (ignoring the terms before the integral sign)

$$f(\theta,\phi) = \int_0^a\int_0^{2\pi} F(\rho,\chi)\exp\left[ik\left\{-\rho\sin\theta\cos(\chi-\phi) + \frac{\rho^2}{2R}\right\}\right]\rho d\rho d\chi. \tag{11}$$

For a rotationally symmetric aperture distribution $F(\rho)$, independent of χ, the integration over χ results in

$$f(\theta) = 2\pi\int_0^a F(\rho)J_0(k\rho\sin\theta)\exp\left(ik\frac{\rho^2}{2R}\right)\rho d\rho. \tag{12}$$

These integrals have been studied by Lommel in his treatment of Fresnel diffraction at a circular aperture and the solution can be written in terms of Lommel functions (for details *c.f.* [Baars (1970)] or [Born & Wolf (1970)]).

In the following we illustrate the near-field by numerically integrating Equation 12[3] We assume the aperture function to be of the form $F(\rho) = 1-(1-\tau)\rho^2$, the "quadratic on a pedestal τ" illumination function with

[3]The calculations and resulting plots of Figures 16 through 20 have been made with the aid of the *Mathematica* package.

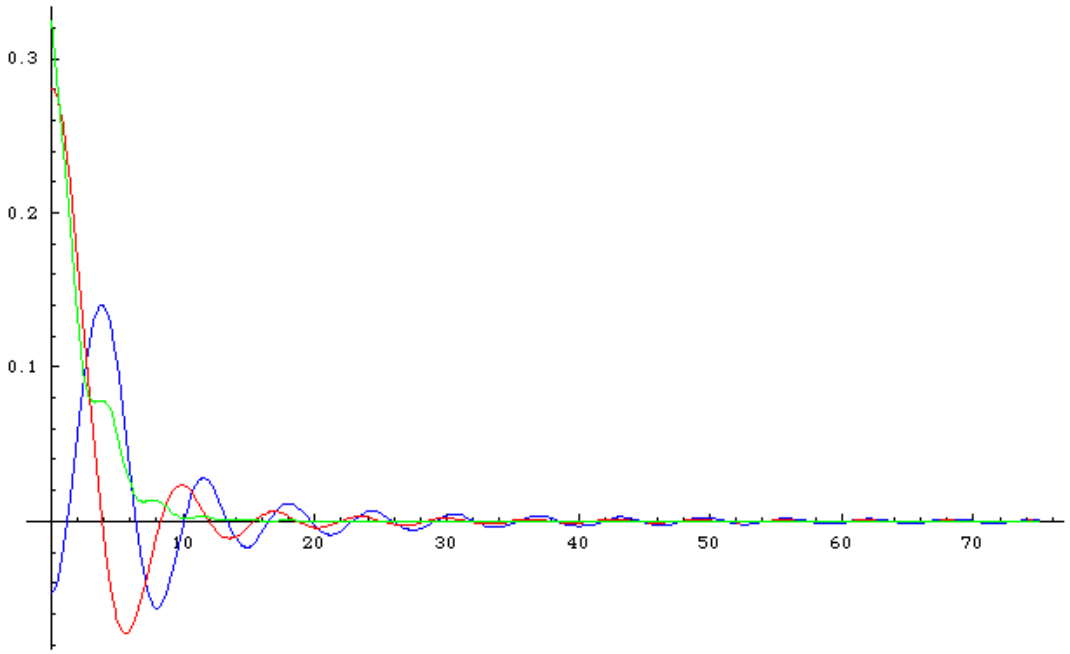

Figure 16: The near-field calculation. Red and blue curves are the sine and cosine-component, respectively, while the green curve is the "powerpattern", i.e. the sum of the squares of the two former (multiplied by a factor 4 for purpose of illustration). This calculation assumes a distance to the aperture of 300 m, wavelength 3 mm and uniform aperture illumination; maximum value of u=75 corresponds with an angle of about 2 degrees off boresight. This numerical example is thus applicable to the holography measurement of the ALMA antennas at the ATF/VLA site.

taper τ (uniform illumination for τ=1). We choose a normalised aperture radius a=1, introduce the variable u=k sin θ and ignore the factor 2π in front of the integration sign. In the integration we must separate the exponent in its cosine and sine part. For uniform illumination, we obtain the result shown in Figure 16.

6.3 The Far-Field Approximation (Fraunhofer Region)

In the **far-field** situation, the field point P is so far away (in principle at infinity) that the vectors $R_1$and $r_1$are parallel and moreover the variation of r in the exponent of Equation 4 can be reduced to the linear form

$$r = R - (u\xi + v\eta) = R - \sin\theta(\xi\cos\phi + \eta\sin\phi). \tag{13}$$

Now, the far-field radiation integral, Equation 4 with $\cos\theta = 1$ can be written as

$$f_P(\theta,\phi) = \frac{i}{\lambda}\frac{e^{-ikR}}{R}\int F(\xi,\eta)\exp\{ik\sin\theta(\xi\cos\phi + \eta\sin\phi)\}\,d\xi d\eta, \tag{14}$$

where the integration is performed over the aperture A. Again applying this equation to a circular, plane aperture with radius **a** and azimuthal angle χ, the integral is transformed into

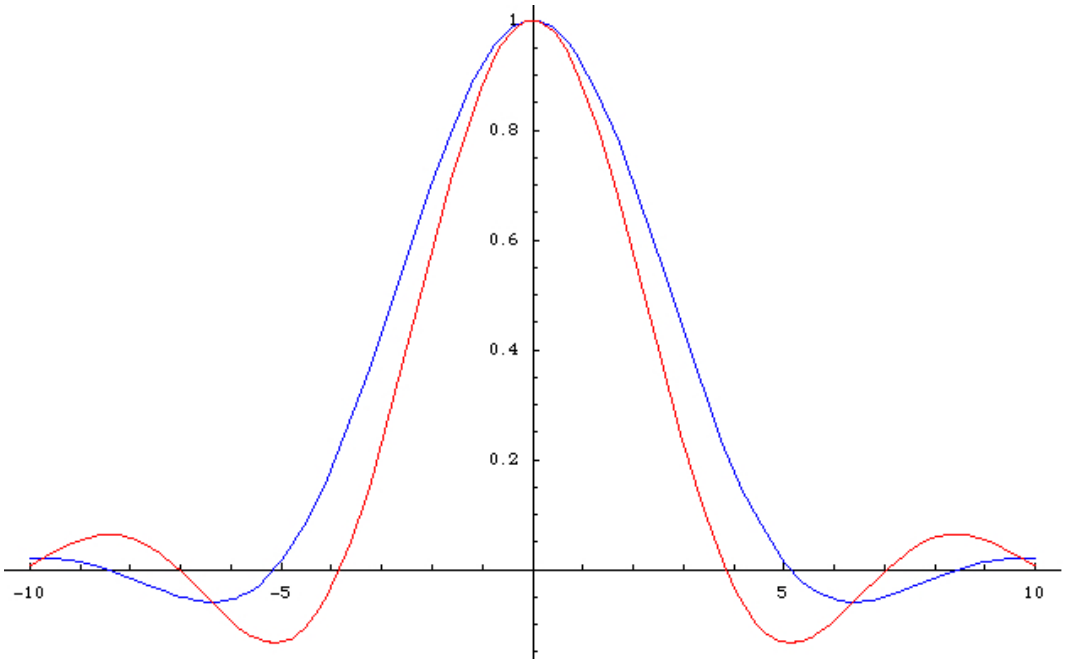

Figure 17: The field pattern for the uniform (red) and fully tapered (blue) illumination function. The tapered case (blue) exhibits a broader beam and lower sidelobes.

$$f(\theta,\phi) = \int_0^a \int_0^{2\pi} F(\rho,\chi) \exp\left[ik\left\{-\rho\sin\theta\cos(\phi-\chi)\right\}\right] \rho d\rho d\chi, \tag{15}$$

which for a rotationally symmetric aperture function $F(\rho)$ takes the form of a Hankel Transform

$$f(\theta,\phi) = 2\pi \int_0^a F(\rho) J_0(k\rho\sin\theta)\rho d\rho \rightarrow 2\pi \frac{J_1(ka\sin\theta)}{ka\sin\theta} = \pi\Lambda_1(ka\sin\theta), \tag{16}$$

where J_0 and J_1 are the Bessel function of the first kind and order zero and one, respectively and Λ_1 is theso-called Lambda function of first order. The expression after the arrow assumes a uniform amplitude distribution $F(\rho) \equiv 1$. Figure 17 presents an illustration of Equation 15 for uniform and tapered illumination.

6.4 The Fourier Transformation Relationship

Using the direction cosines (u,v), introduced above after Equation 5, Equation 14 can also be written as

$$f_P(u,v) = \frac{i}{\lambda}\frac{e^{-ikR}}{R} \int F(\xi,\eta) \exp\{ik(\xi u + \eta v)\} d\xi d\eta \tag{17}$$

and we see that there is a fourier transformation relationship between $f(u,v)$ and $F(\xi,\eta)$.

Ignoring the term in front of the integral sign, the **inverse Fourier transformation** can now be written as

$$F(\xi,\eta) = \int f(u,v)\exp\{-ik(u\xi+v\eta)\}dudv, \tag{18}$$

where the integration in principle has to be performed over a closed surface, surrounding the aperture. Thus a knowledge of the entire far-field pattern **both in amplitude and in phase** provides a description of the complex field distribution over the aperture of the antenna, also in amplitude and phase.

It is interesting to note that Silver devotes a lengthy discussion to this relationship (Ch. 6.3, 1949), but concludes that the practical application is limited by the fact that the far-field pattern is only prescribed in power. Thus the phase function of $f(\theta,\phi)$ would be arbitrary and the aperture distribution cannot be uniquely determined. It was, as noted in the introduction, Jennison who mentioned the same relation and its practical usefulness, pointing out that the amplitude and phase can both be measured with an interferometer. When Silver wrote his text in the mid forties, radio interferometry had not yet been developed.

In most cases it will be impossible, or in any case impractical, to measure the far-field pattern over the entire sphere. It can be shown however that a measurement of the pattern out to an angle Θ = n Θ_A from the beam axis yields the aperture distribution with a spatial resolution of $\delta = \frac{D}{n}$, where $\Theta_A \approx \frac{\lambda}{D}$ is the half-power beam width and D is the aperture diameter, λ the wavelength.

6.5 Mathematical Details of Near-Field Holography

We now continue with the treatment of holography in the nearfield. Because we want to derive the complex aperture distribution form the measured near-field pattern, the inverse Fourier Transformation of Equation 4 will be our point of departure, where Equation 5, but now written with direction cosines(u,v), is the expression for the finite distance from a point in the aperture to the field point P. Thus we have the inverse of Equation 4

$$F(\xi,\eta) = \frac{i}{\lambda R}\int f(u,v)\exp(-ikr)dudv. \tag{19}$$

Note that we have assumed that the angle θ is small enough to allow cos θ to be set to unity (<0.1 percent error for θ up to 3 degrees). R is the distance from the antenna aperture center to the holography signal source. From the discussion in the foregoing section we repeat here the series expansion for the distance **r** (Equation 9):

$$r \approx R - (u\xi+v\eta) + \frac{\xi^2+\eta^2}{2R} - \frac{(\xi^2+\eta^2)^2}{8R^3} - \frac{(u\xi+v\eta)^2}{2R} + \frac{(\xi^2+\eta^2)(u\xi+v\eta)}{2R^2}. \tag{20}$$

As noted above, normally for the Fresnel region analysis, the series is stopped after the quadratic term, which preserves the first three terms in Equation 20. Here, we shall maintain the next terms too in order to make an estimate of the error in the approximation. Substitution of Equation 20 into Equation 19 yields

$$F(\xi,\eta) = \frac{i}{\lambda}\frac{e^{-ikR}}{R}\exp\{-ik\delta p_1(\xi,\eta)\}\int f(u,v)\exp\{ik(u\xi+v\eta)\}e^{-ik\epsilon}dudv. \tag{21}$$

The terms in Equation 20, which are independent of the integration variables, have been brought outside the integral under the variable δp_1. The other terms in higher powers of (u,v) are collected under the variable ϵ. They "modify" the direct Fourier Transformation of Equation 21. The first pathlength term

$$\delta p_1(\xi,\eta) = \frac{\xi^2+\eta^2}{2R} - \frac{\left(\xi^2+\eta^2\right)^2}{8R^3} \tag{22}$$

causes a rapidly varying phase variation over the aperture, which can be compensated to a large degree by an axial displacement of the feed. A focus adjustment δf away from the reflector causes a path length variation of

$$\delta p_2(\xi,\eta) = \left\{\xi^2+\eta^2+\left(f-\frac{\xi^2+\eta^2}{4f}+\delta f\right)^2\right\}^{0.5} - \left\{f+\frac{\xi^2+\eta^2}{4f}+\delta f\right\}. \tag{23}$$

In Figure 18 we illustrate the behaviour of these terms as function of the radial aperture coordinate. The "cosine component" of the phase function of Equation 22 for 3mm wavelength and a distance R = 300 m is shown in red, while the phase function of Equation 23 for a certain choice of δf is superposed in blue. The difference between both terms is shown in the lower plot. Clearly, the phase error increases its spatial frequency for increasing radial aperture coordinate. The difference plot shows that the residuals are significant for the outer half of the aperture. By varying the value of δf, one can obtain an impression of its influence on structure and magnitude of the difference function (Figure 19).

We want to minimise the sum of the two terms (Equations 22 and 23) by choosing the appropriate value of δf. Because of the (ξ,η)-dependence (as shown above), there will be a residual path length error, which we must apply to the result of the Fourier Transformation. A value of 102 mm seems the most useful for R = 300 m. The remaining error must be introduced in the mathematical analysis of the data according to the curve. This is a correction to the aperture phase distribution, obtained after the Fourier Transformation of the measured beam pattern.

The higher order terms in Equation 20, containing the integration variables (u,v), must be discussed separately. They constitute a small pathlength error

$$\epsilon = \frac{\left(\xi^2+\eta^2\right)(u\xi+v\eta)}{2R^2} - \frac{(u\xi+v\eta)^2}{2R}, \tag{24}$$

which adds a phase term to the integral of Equation 19 of the following form

$$\exp(-ik\epsilon) \approx 1 - ik\epsilon = 1 - ik\left\{u\frac{\xi(\xi^2+\eta^2)}{2R^2} + v\frac{\eta(\xi^2+\eta^2)}{2R^2} - u^2\frac{\xi^2}{2R} - v^2\frac{\eta^2}{2R} - uv\frac{\xi\eta}{R}\right\}. \tag{25}$$

It is seen that this correction involves the calculation of five additional integrals, which look like Fourier Transformations, but aren't really *bona fide* FTs.

The magnitude of the remaining term ϵ (Equation 24) is illustrated in Figure 20.

At the edge of the measured beam the largest path length error is about −0.4 mm at one edge of the aperture. Let us look at some other numerical values for the case of the ALMA antennas. Here the distance R = 300 - 315 m; the reflector diameter is 12 m, so maximum value of (ξ , η) = 6 m. For a beam map with 180 points across a scan, we obtain a resolution in the aperture of about 15 cm, which is fully suitable for the interpolation of the adjuster settings. The scan angle in this case is about plus and minus 1.5 degrees. This means the maximum value of the direction cosines (u,v) $\approx$ 0.03.

Thus the maximum value of the components of Equation 22 become

$$\begin{aligned}\delta p_1 &= \frac{72}{600} - \frac{(72)^2}{(8*(300)^3)} \\ &= 0.12 - 0.24\times10^{-4}.\end{aligned}$$

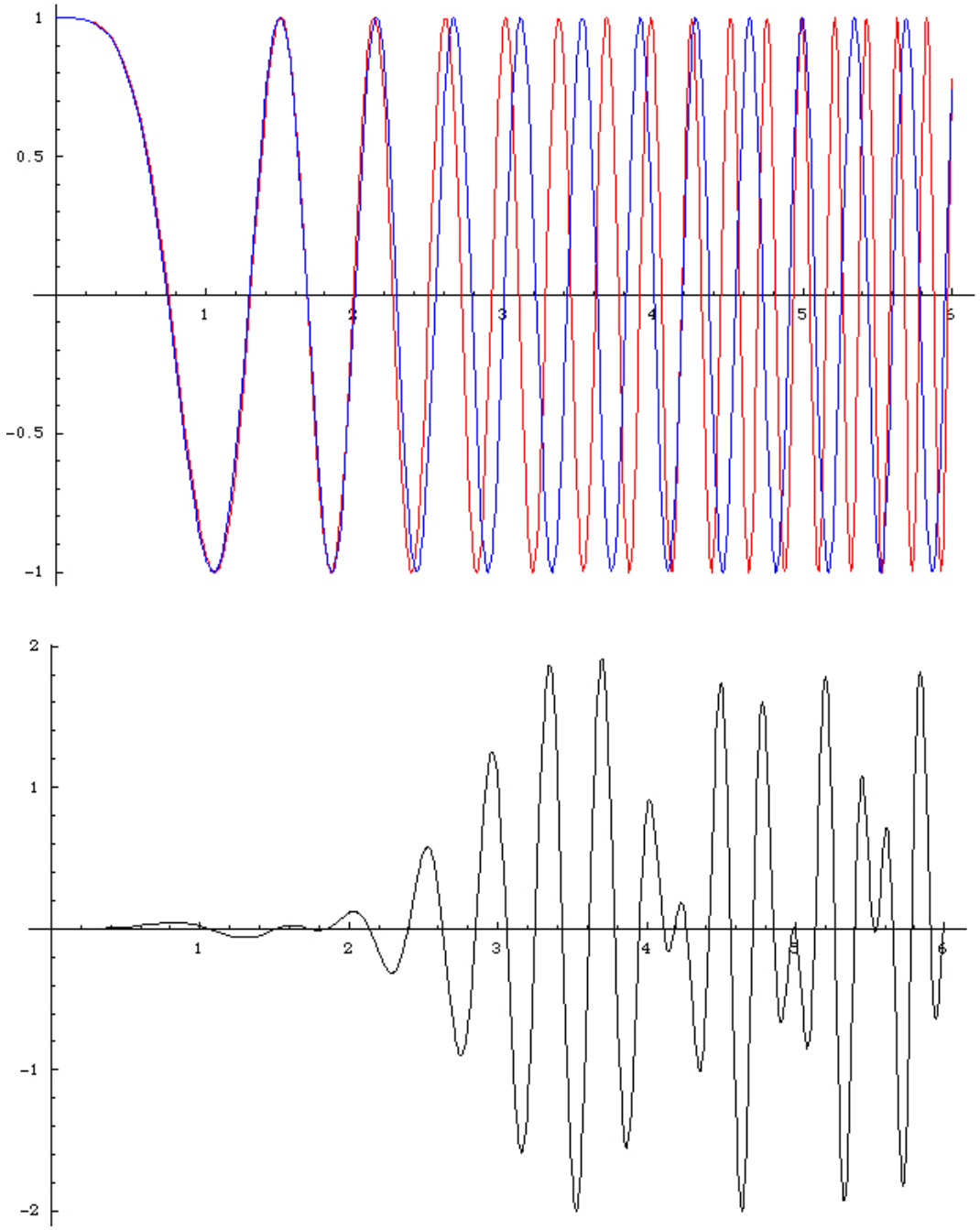

Figure 18: Residual aperture phase for finite distance and axial defocus. Top: Eq.(20), red, and Eq.(21), blue. The lower curve shows the differenceof the two.

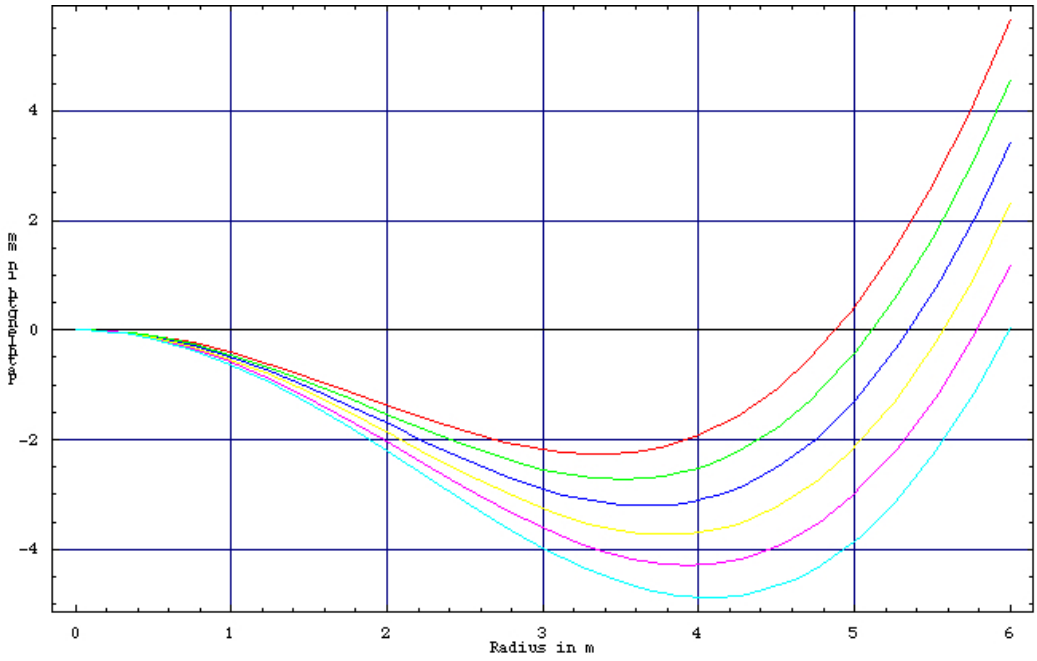

Figure 19: The residual pathlength error in mm for a distance R = 300 m to the holography transmitter and the ALMA 12-m diameter antenna with $\frac{f}{D} = 0.4$. The parameter is the axial defocus δf = 96, step 2, 106 mm, from top to bottom.

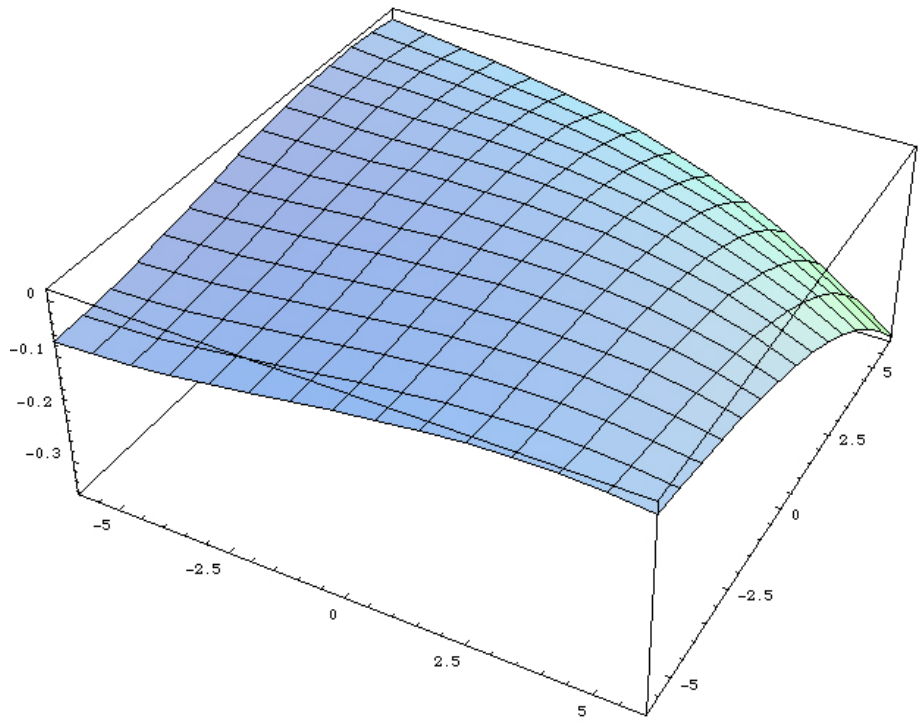

Figure 20: A three-dimensional illustration of the second order path error corrections (Equation 24).

The last term is 5000 times smaller than the first and normally fully negligible. The maximum magnitude of ϵ is

$$\begin{aligned}\epsilon &= \frac{72 * 0.36}{(2 * (300)^2)} - \frac{(0.36)^2}{600} \\ &= 14 \times 10^{-5} - 21.6 \times 10^{-5} \\ &= -8 \times 10^{-5}.\end{aligned}$$

Compare this term with the main term in the Fourier transform (uξ+vη) (Equation 19), which attains a maximum value of 0.36, *i.e.* 4500 times larger.

Nevertheless, because these terms influence the phase over the aperture, they must be dealt with carefully. When all the integrals of Equation 24 are evaluated, it turns out that the contribution of ϵ to the phase amounts to 2 μm pathlength over most of the aperture, reaching a value of 5μm at the edge[4]. In a high accuracy measurement, where the aim is to achieve a measuring accuracy of better than 10 μm, one might indeed correct for this term.

As stated above, the near-field path length error of Equation 22 is compensated as well as possible by an axial defocus of the feed (Equation 23). The remaining path error, as depicted, attains values of several millimeters and a correction over the aperture must be applied in all cases. As mentioned earlier, this is easily done by direct addition to the derived aperture distribution after the Fourier Transformation.

It is possible that during the measurement the receiver feed is not located in the optimum refocused position. The pathlength error caused by an axial defocus of δz follows from Equation 23 as

$$\delta p_z = \delta z \left\{ 1 - \frac{1 - \frac{\xi^2+\eta^2}{4f^2} + \frac{\delta f}{f}}{\sqrt{\frac{\xi^2+\eta^2}{4f^2} + \left(1 - \frac{\xi^2+\eta^2}{4f^2} + \frac{\delta f}{f}\right)^2}} \right\}, \tag{26}$$

while a transverse (lateral) offset by an amount δx will cause a pathlength variation of

$$\delta p_x = \delta x \frac{\xi}{f} \left\{ \frac{1}{1 + \frac{\delta f}{f}} - \frac{1}{\sqrt{\frac{\xi^2+\eta^2}{f^2} + \left(1 - \frac{\xi^2+\eta^2}{4f^2} + \frac{\delta f}{f}\right)^2}} \right\}. \tag{27}$$

In the reduction process of the holography data, these terms are found by a fit of the measured beam map. The final map of surface deviations is then referred to a position of the feed in the fitted "out-of-focus" location.

6.6 Practical Realisation of the Holography Measurements

6.6.1 Task

In this chapter we describe the way in which a holography measurement has been executed on the ALMA prototype antennas at the VLA site. The specification requires the antennas to have a surface accuracy of 25μm RMS for the AEC antenna (with a goal of 20μm) and 20μm for the VertexRSI antenna. ALMA assumed the task to demonstrate this with the aid of a holography system at 3 mm wavelength after delivery of the

[4]This is shown in Figure 21.

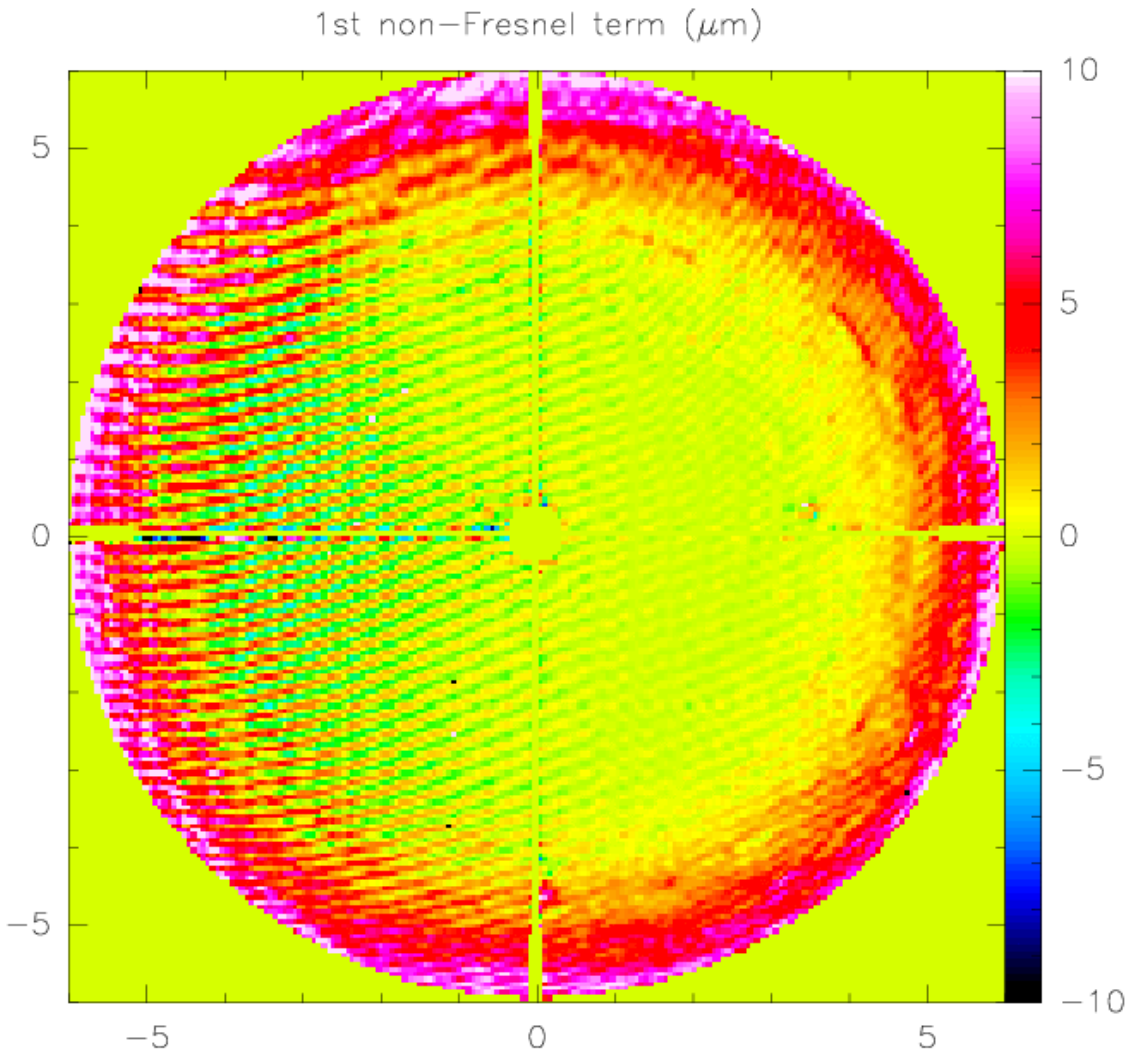

Figure 21: Non-Fresnel correction terms.

antennas by the contractors with a surface accuracy of not worse than 100μm RMS. This initial setting was performed by VertexRSI with digital photogrammetry and by AEC with the aid of a Leica "total station" laser-tracker (basically a theodolite with integrated distance measurement instrument and all-electronic readout).

The holography system was designed to provide a measurement repeatability of 10μm, which would suffice to demonstrate the realism in the obtained overall surface accuracy. It should be noted that in the current setup the holography system provides a surface map at one elevation only. No information on the gravitational deformation of the antenna with varying elevation angle can be obtained.

6.6.2 Equipment and Execution of the Measurement Program

— The signal source for the holography measurements is a monochromatic transmitter at a frequency of 78.92 or 104.02 GHz, located on a 50 m high tower at a distance of 315 and 302 m from the Vertex and AEC antenna, respectively.
— The elevation angle is approximately 8 degrees. The receiver is a full-phase double-receiver, located in the apex region behind the primary focus of the main antenna. The reference signal is received by a wide beam horn pointing along the boresight towards the transmitter.
— Amplitude and phase maps of the antenna beam were obtained by raster scanning. After Fourier Transformation a map of the aperture amplitude and phase distribution was obtained with a spatial resolution over the aperture of about 0.15 m. A typical measurement takes about one hour of time.
— From the phase distribution, which is a representation of the misalignment of the 264 (VertexRSI) or 120 (AEC) panels constituting the reflector, the necessary adjustments of the 5 support points per panel were derived. These were then applied by hand with a simple tool to improve the accuracy of the reflector surface.

The algorithms and software used for the data analysis and derivation of the panel adjustments have been applied successfully at the telescopes of IRAM. The necessary corrections for the finite distance to the transmitter (the "near field" corrections) in our case were derived and checked against similar corrections applied by others, *e.g.* for the JCMT.

The equipment has been designed to provide sufficient signal–to–noise ratio to render the error due to noise insignificant. The greatest risk in this type of measurements lies in undetected or poorly corrected systematic errors.

— An accurate knowledge of the amplitude and phase function of the feedhorn, illuminating the reflector, is essential, because errors in these are fully transferred to the aperture phase map and hence to the surface profile.
— Multiple reflections from the ground or structures form a possible source of errors in this type of work. We carefully covered all areas of potentially harmful reflections with absorbing material. In some controlled experiments we could not demonstrate the existence of reflections.
— The dynamic range of the receiver must be sufficient to accommodate the strong signal on the peak of the beam and the very weak signals towards the edge of the scan. There might have been some saturation on some of the measurements. We discuss this in more detail below.
— The effect of the finite distance of the transmitter can be removed to a large extent (but not completely) by an axial shift in the position of the feed. An error in the distance to the transmitter thus can be corrected in the data analysis by a small adjustment of the feed position. The remaining phase error can be accurately calculated and applied to the data.

A Some Useful Equations and Calculations

A.1 Definitions

$c \equiv$ speed of light

$\lambda \equiv$ observing wavelength

$f_1 \equiv$ taper factor for signal feed

$f_{apo} \equiv$ apodization smoothing factor

$f_{osr} \equiv$ map oversampling factor between rows

$f_{oss} \equiv$ map oversampling factor along a row

$D \equiv$ main antenna diameter

$d \equiv$ reference feed diameter

$\theta_{ext} \equiv$ angular extent of map (assumed square, in radians)

$\theta_b \equiv$ primary beam size (radians)

$\theta_{sr} \equiv$ sampling interval between rows (radians)

$\theta_{ss} \equiv$ sampling interval along a scan (radians)

$N_{row} \equiv$ number of rows in map

$\delta_d \equiv$ spatial resolution on dish

$\dot{\theta} \equiv$ map row scanning rate

$L_m \equiv$ linear size of map

$P \equiv$ Transmitter EIRP

$P_r \equiv$ Reference feed power received

$P_s \equiv$ Main antenna power received on boresight

$B \equiv$ Detector bandwidth

$t_{int} \equiv$ Integration time

$\alpha \equiv$ Scan angle, which ranges from $-\frac{\theta_{ext}}{2}$ to $+\frac{\theta_{ext}}{2}$

$R \equiv$ Distance between holography transmitter and receiver

$\Delta z \equiv$ Reflector surface displacement accuracy

A.2 Map Resolution and Sampling

$$\begin{aligned} \theta_b &= \frac{f_1 c}{\nu D} \\ &= \frac{61836.6 f_1}{\nu(GHz) D(m)}\ arcsec \end{aligned} \tag{28}$$

$$\begin{aligned}\theta_{sr} &= \frac{\theta_b}{f_{osr}} \\ &= \frac{f_1 c}{f_{osr}\nu D} \\ &= \frac{61836.6 f_1}{f_{osr}\nu(GHz)D(m)}\ arcsec \end{aligned} \tag{29}$$

$$\begin{aligned}\theta_{ss} &= \frac{\theta_b}{f_{oss}} \\ &= \dot{\theta} t_{samp} \\ &= 0.012\dot{\theta}\ arcsec \end{aligned} \tag{30}$$

$$\begin{aligned}\delta_d &= \frac{D}{N_{row}} \\ &= \frac{f_1 f_{apo} c}{\nu\theta_{ext}} \\ &= \frac{1717.7 f_1 f_{apo}}{\nu(GHz)\theta_{ext}(deg)}\ cm \end{aligned} \tag{31}$$

$$\begin{aligned}t_{map} &= N_{row} t_{row} \\ &= \frac{f_{osr}\theta_{ext}^2}{\dot{\theta}\theta_b} \\ &= \frac{1717.7 \times 10^2 f_{osr} f_1 D(m)}{\dot{\theta}(''/sec)\nu(GHz)\delta_d^2(cm)}\ hours \end{aligned} \tag{32}$$

A.3 Power, Noise, and Sensitivity

$$\begin{aligned}P_r &= \frac{\pi d^2}{4}\frac{P}{4\pi R^2} \\ &= \frac{1}{16}\left(\frac{d}{R}\right)^2 P \end{aligned} \tag{33}$$

$$\begin{aligned}P_s &= \frac{\pi D^2}{4}\frac{P}{4\pi R^2} \\ &= \frac{1}{16}\left(\frac{D}{R}\right)^2 P \end{aligned} \tag{34}$$

$$P_s(\alpha) = P_s(0)\left[\frac{J_1\left(\frac{\pi\alpha D}{\lambda}\right)}{\left(\frac{\pi\alpha D}{2\lambda}\right)}\right]^2 \tag{35}$$

$$\sigma^2 = \frac{\left[kT_{sys}B + P_r + P_s(\alpha)\right]kT_{sys}}{t_{int}} \tag{36}$$

$$\begin{aligned}\delta z &= \frac{\lambda}{16\sqrt{2}}\frac{\sqrt{N_{sx}N_{sy}}}{f_{os}^2}\frac{\sigma_{av}}{M_0} \\ &= 0.044\lambda\frac{\sqrt{N_{sx}N_{sy}}}{f_{os}^2}\frac{\sigma_{av}}{M_0}\end{aligned} \tag{37}$$

For our holography system:

1. $t_{int} = 36$ msec,
2. $M_0 = \sqrt{P_s(0)P_r} = 4.167 \times 10^{-7}$P,
3. $\sigma_0 = \left(1.23 \times 10^{-22}W(P)\right)^{\frac{1}{2}}$,
4. P_r Term $= \left(2.13 \times 10^{-27}W(P)\right)^{\frac{1}{2}}$
5. Average map noise for complex correlator $(\sigma_{av}) = \left(2.23 \times 10^{-25}W(P)\right)^{\frac{1}{2}}$,
6. $\delta z = \frac{1.35\times10^{-2}}{\sqrt{P}}$

Thus, if we want an error in the measurement of the surface shape of $\delta z = 5$ μm, we need a transmitter with an EIRP of P = 7.3 μW. The expected radiated power is in excess of 10μW, so there is a good margin. Noise will not be the limiting factor in the accuracy of the measurement.

B Panel and Screw Numbering System

The same system for numbering the panels and screws were used for both the VertexRSI and AEC antennas. Panels are referenced as `ss-rp`, where:

— `ss` = Sector number, There are as many sectors as panels in inner ring (12).
They are numbered 01 to 12 starting from right, anti-clockwise, when looking at the primary reflecting surface from the primary focus.
— `r` = ring number, from 1 (inner) to 8 (VertexRSI outer) or 5 (AEC outer).
— `p` = panel position – 1 to 4, anti-clockwise from the same viewpoint, in sector `ss` along ring `r`.
— On each panel, there are five adjusting screws, numbered 1 to 5:
  — 1 and 2 are on the inner side (closest to the center of the dish).
  — 3 and 4 are on the outer side (closest to the edge of the dish).
  — 1 and 3 are on the panel left edge when looking from the primary focus, 2 and 4 on the right side.
  — 5 is at or near the center of the panel.

Positive screw settings mean that the panel has to move closer to the primary focus ("up").

Figure 22 shows the panel numbering system for the VertexRSI antenna, while Figure 23 shows the panel numbering system for the AEC antenna. Figure 24 shows the screw numbering system for an individual panel on both antennas.

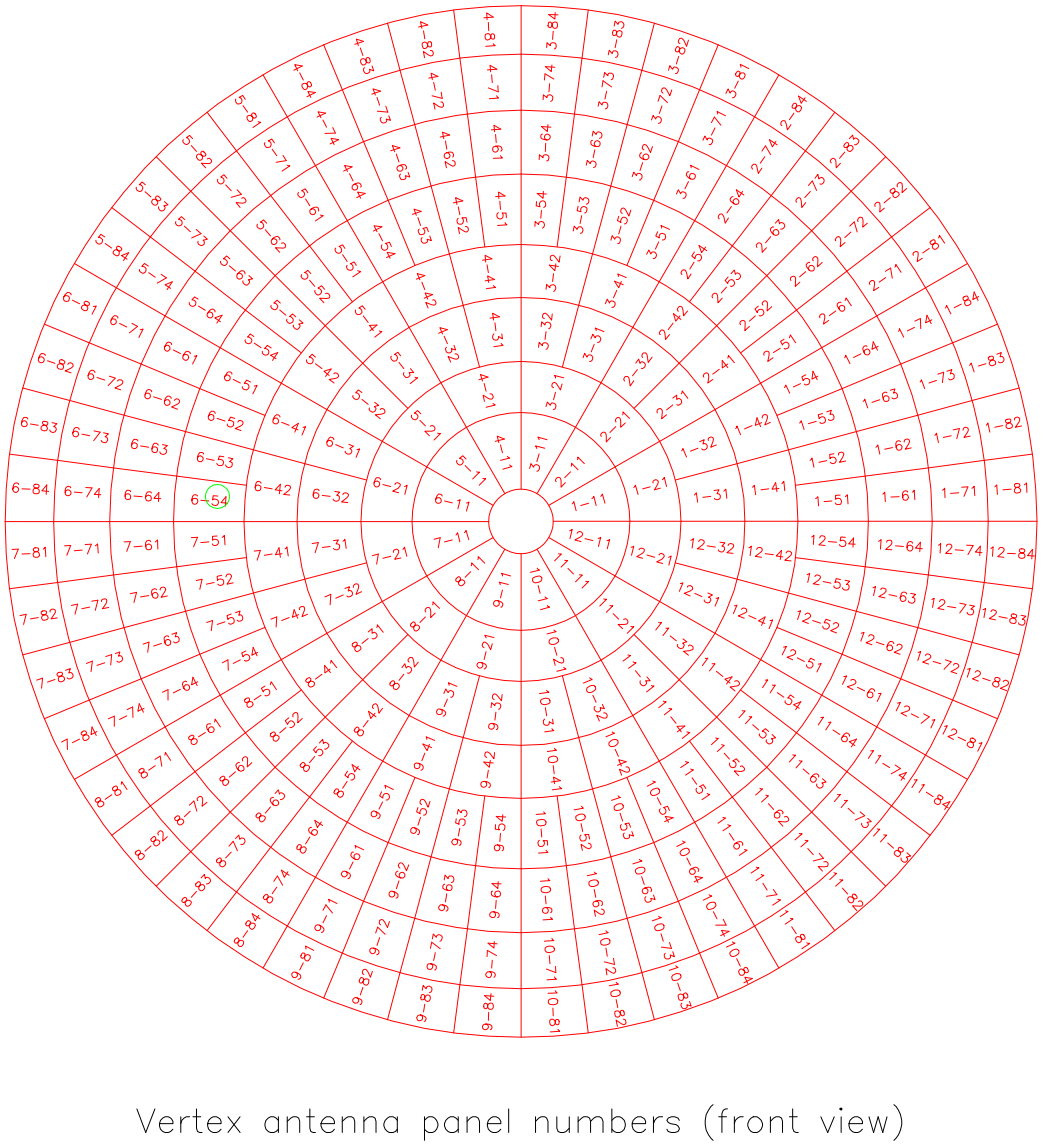

Figure 22: Panel numbering layout for the VertexRSI antenna. The green circle marks the position of the access hole for the optical pointing telescope.

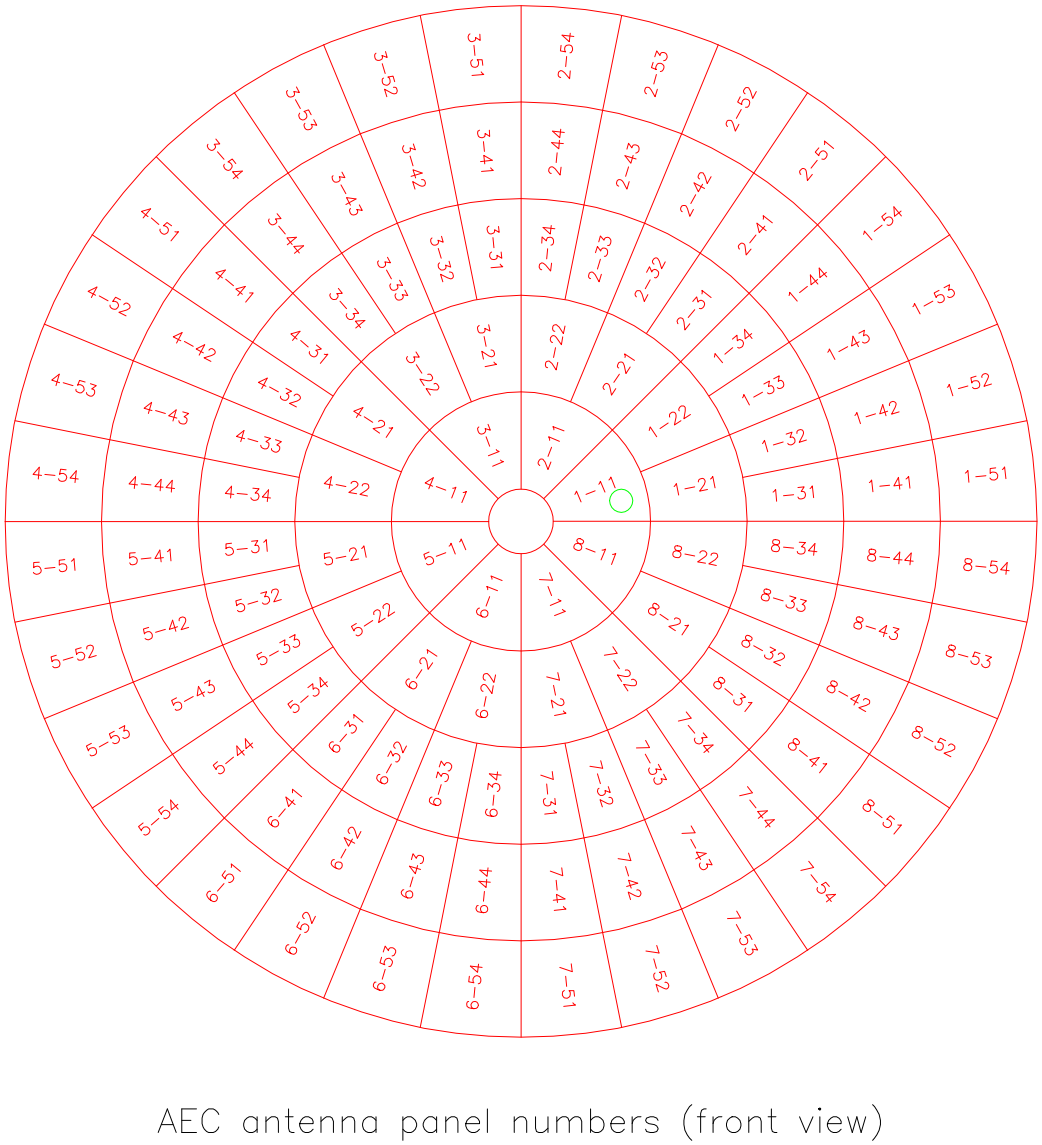

Figure 23: Panel numbering layout for the AEC antenna. The green circle marks the position of the access hole for the optical pointing telescope.

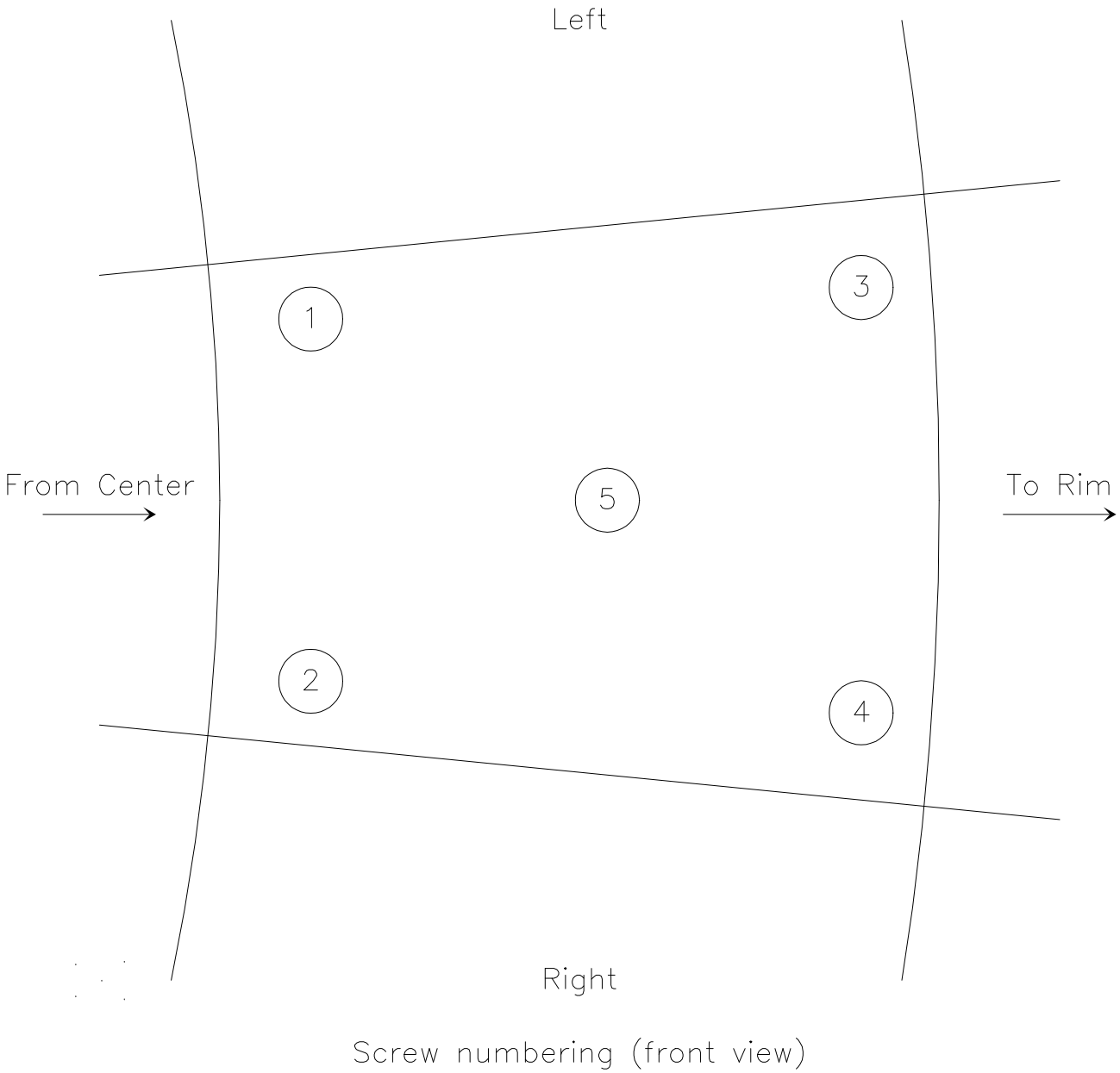

Figure 24: Screw numbering system used for each panel on both the VertexRSI and AEC antennas.

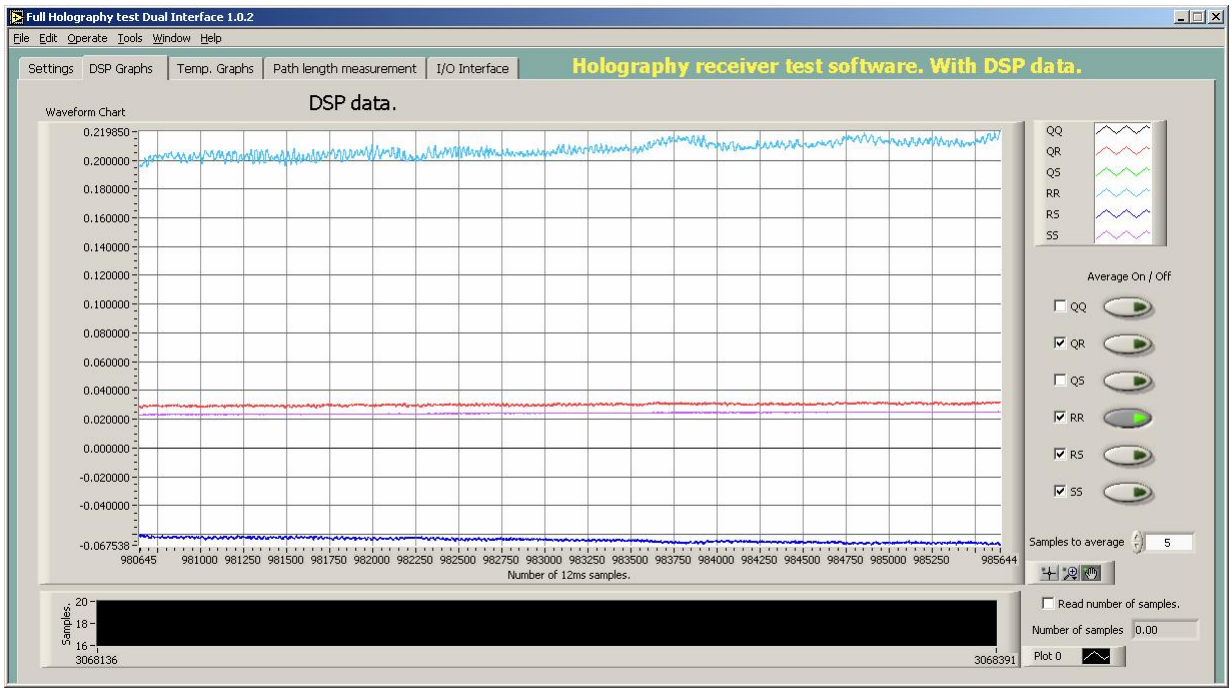

Figure 25: Oscillation in amplitude of the R*R signal at the receiver. The frequency is about 1.25 Hz and the amplitude is 2 or 3%. The oscillation comes and goes randomly.

C Tower Oscillation Test

November 4 2006 (DTE and JGM)

We noted quite frequent oscillations in amplitude, which come and go at unpredictable times. The amplitude peaks at nearly 5% peak-to-peak, and the period is about 1.25 Hz. An example is shown in Figure 25

Antonio suggested this may be a tower oscillation. We were able to force the oscillation of amplitude by "twanging" the far guy wire on the tower, which is in line with the tower and the VertexRSI antenna at the ATF. Twanging one of the other two tower guys did not appear to induce the oscillation. Figures 25, 26, and 27 show this effect.

Conclusion: There is a roughly $\sim 2\%$ oscillation in amplitude of the received signal, which is seen strongly correlated in both reference and signal receiver channels. A very likely cause is tower oscillation; the observed effect can be induced by "twanging" the far tower guy. The tower oscillation may be turned into amplitude modulation by some kind of multipath reception. A quick test was made to see if a reflection from the ground was responsible, but as the antenna was moved away from the transmitter antenna towards the possible reflection point, the oscillation disappeared. If this is multipath, the reflection point is unknown.

The effect on holography is to add an extra source of noise, of about ~ 2 μm rms. This is probably small enough not to be a serious concern.

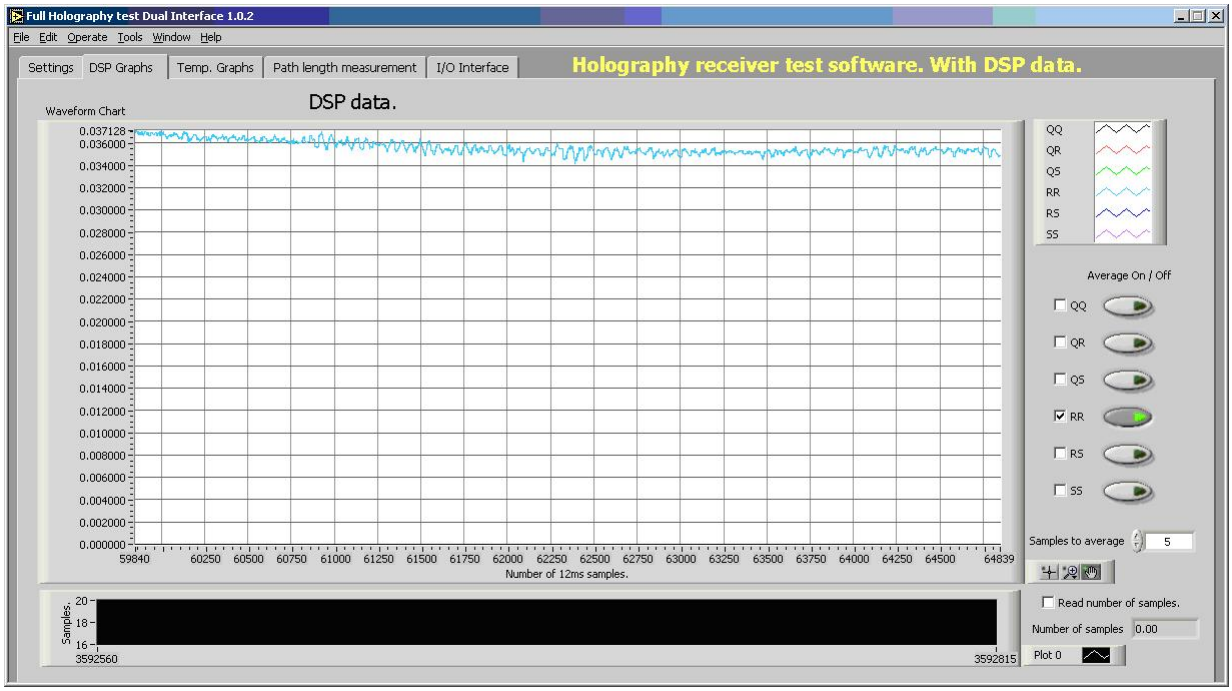

Figure 26: Plot of "R*R" or reference power from receiver DSP (upper, blue line). Note the regular oscillation of nearly 5% in amplitude, with a period of about 1.25 Hz. This example was caused to happen by "twanging" the far guy wire of the tower, but is similar to effects seen at other times such as in Figure 25 – caused presumably by tower oscillation.

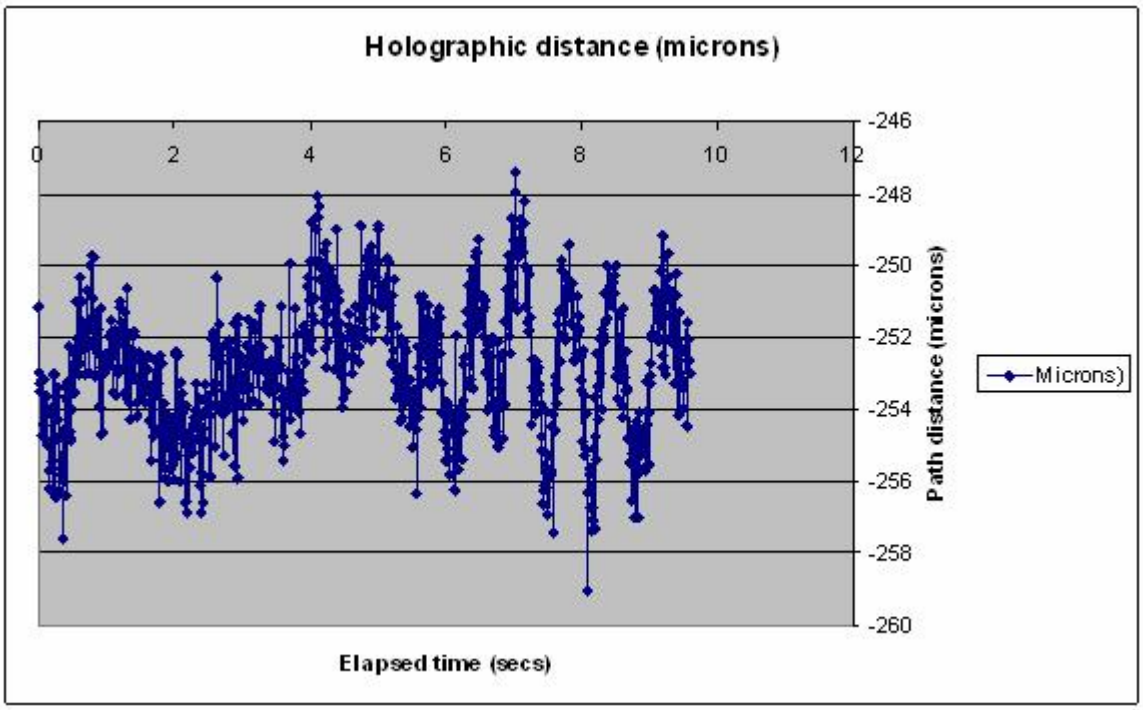

Figure 27: The phase (interpreted as a distance) observed during an amplitude oscillation, similar to but not simultaneous to Figure 25. The peak-to-peak oscillation is equivalent to about ± 3 μm, is roughly sinusoidal so has an rms value of about 2 μm.

D Measurement of Holography Receiver Linearity

November 11, 2006 (DTE and JGM)

The linearity of the holography receiver was measured, using the holography transmitter, in two different experiments.

1. By first setting the transmitter at relatively high power (+8 dBm on the Synthesizer Power Level of the Holography Transmitter Monitor and Control). See Figure 28; then varying the attenuators within the receiver control (see Figure 29) and noting the output of the receiver as measured by the IF volts ("REF I" "REF Q" "SIG I" and "SIG Q" channels in Figure 29), and also as measured on the DSP Graphs by R*R and S*S, displayed in the same Labview program. This process measures the linearity of the receiver beyond the point where the attenuators are located.
2. By choosing a receiver operating point (setting the Ref and Sig attenuators) where the operation is very linear, and then using the Transmitter Synthesizer to vary the power input. The 1 dB steps on the synthesizer correspond to approximately 6 dB at the output of the synthesizer. A fixed change of receiver input was then applied by offsetting the antenna pointing from boresight; a constant signal change of approximately 1 dB was obtained by this antenna pointing offset. The magnitude of that fixed change of amplitude was then measured as the transmitter power output was varied over a range of approximately 20 dB, by varying the Transmitter Synthesizer output level.

The receiver attenuators were then changed (see "Attenuators" in Figure 29.)

D.1 Receiver Linearity After the Attenuators

Table 4 shows the measured values of the Reference Receiver, which are plotted in Figure 30. The transmitter synthesizer output was set to +8 dBm, which is about the highest level at which stable transmitter operation can be guaranteed. The final conclusion is that the receiver measured this way is quite linear with attenuator settings of at least 8 dB, with this particular level of transmitter power. From Table 4, this corresponds to a RefI and RefQ channel voltage of about 13 volts. This is consistent with previous laboratory measurements of the receiver

Table 4 shows measurements of receiver output as a function of dB settings of the Reference receiver. "Rx dB" shows the values of attenuation entered in the Labview window shown in Figure 29. Ref I and Ref Q were measured from the channel voltages displayed in the Labview window shown in Figure 29. R*R was measured from the graphical display of "DSP Graphs" of the same program. The columns dBRefI, dBRefQ and dBR*R are dB values calculated from RefI RefQ and R*R, normalized to 0 dB with 30 dB of receiver attenuation. The final column is just calculated as "30 dB – Rx dB" to give the expected plot of a perfect system.

Table 5 shows the corresponding measurements for the Main Signal Receiver, with Figure 31 showing a plot of the measurements.

Figure 31 shows that no significant non-linearity occurs at any level of main signal receiver attenuation, with this level of transmitter power. The deviations between 5 and 10 dB are believed to result from a drift in transmitter power output during the measurements. So, for the main signal receiver, a receiver attenuation of 0 dB will give the best signal-to-noise ratio, for this level of transmitter power. This corresponds to about 6 dB below the onset of non-linearity, if the receiver behaves in a similar way to the reference receiver shown in Figure 30.

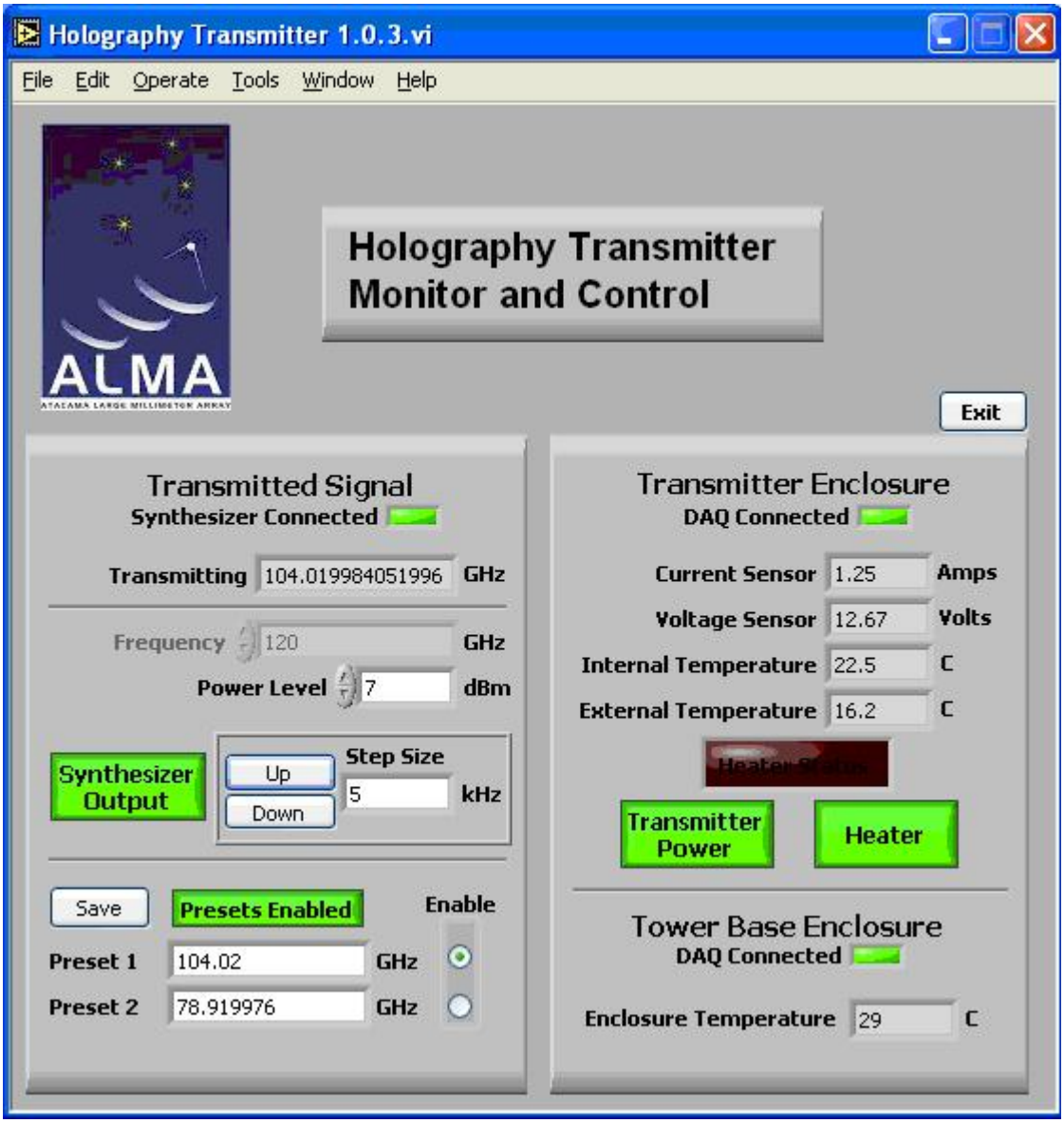

Figure 28: Holography Transmitter Monitor and Control. The Synthesizer Output is used to control the transmitter power output (set at +7 dBm in the figure). Because the synthesizer drives a X6 multiplier, 1 dB change of the synthesizer output produces approximately 6 dB change in actual transmitter output.

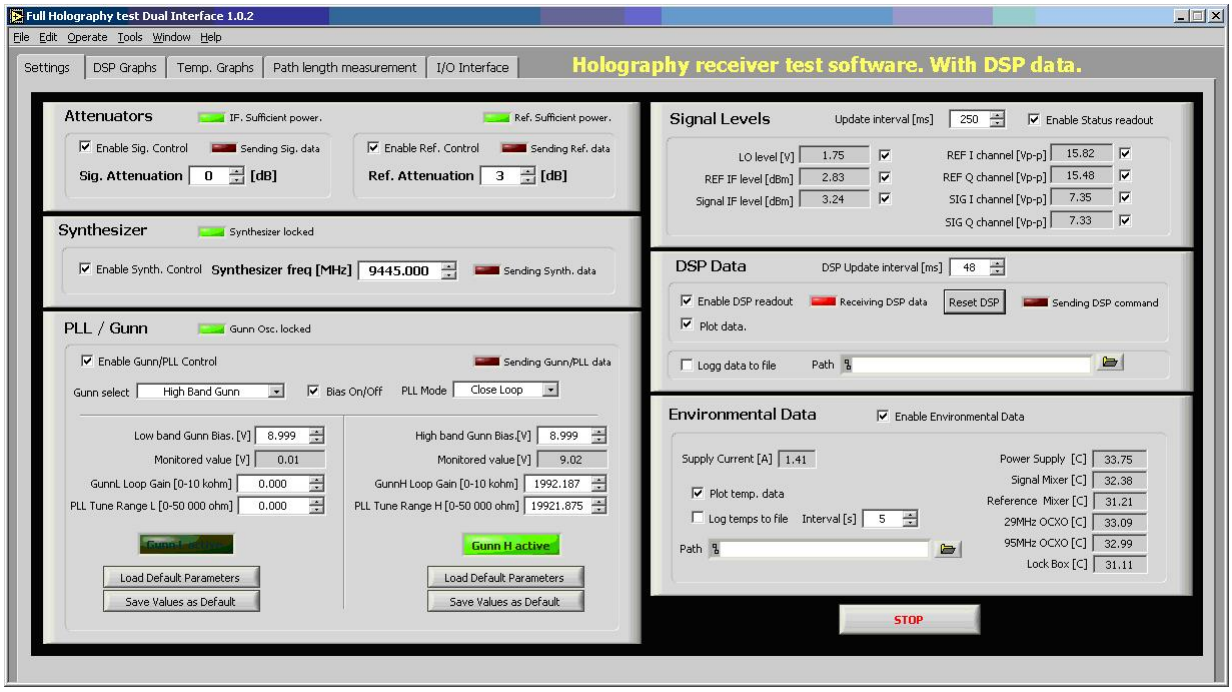

Figure 29: The Holography receiver Labview test software. Receiver attenuators can be varied independently for the signal channel and reference channel. These attenuators ("Sig. Attenuation" and "Ref. Attenuation" in the above window) are located in the 30 MHz chain after the first mixer and some RF amplification within the receiver.

Table 4: Holography Reference Receiver Linearity Measurements

Rx dB	Ref I	Ref Q	R*R	dBRefI	dBRefQ	dBR*R	30 – Rx dB
30	0.88	0.86	0.00065	0	0	0	0
25	1.52	1.51	0.00194	4.747218	4.88957	4.748884	5
20	2.74	2.66	0.0058	9.865358	9.807664	9.505146	10
15	5.18	5.08	0.022	15.39694	15.42731	15.29509	15
10	10.13	10	0.081	21.22254	21.31003	20.95572	20
9	11.61	11.3	0.106	22.40699	22.3716	22.12393	21
8	13	12.8	0.135	23.38921	23.45423	23.1742	22
7	14.9	14.6	0.178	24.57407	24.59709	24.37507	23
6	16.8	16.4	0.22	25.61653	25.60691	25.29509	24
5	18.3	17.8	0.26	26.35937	26.31843	26.0206	25
4	20	19.8	0.255	27.13095	27.24333	25.93627	26
3	20	20	0.225	27.13095	27.33063	25.39269	27
2	20	20	0.215	27.13095	27.33063	25.19525	28
1	20	20	0.22	27.13095	27.33063	25.29509	29
0	20	20	0.18	27.13095	27.33063	24.42359	30

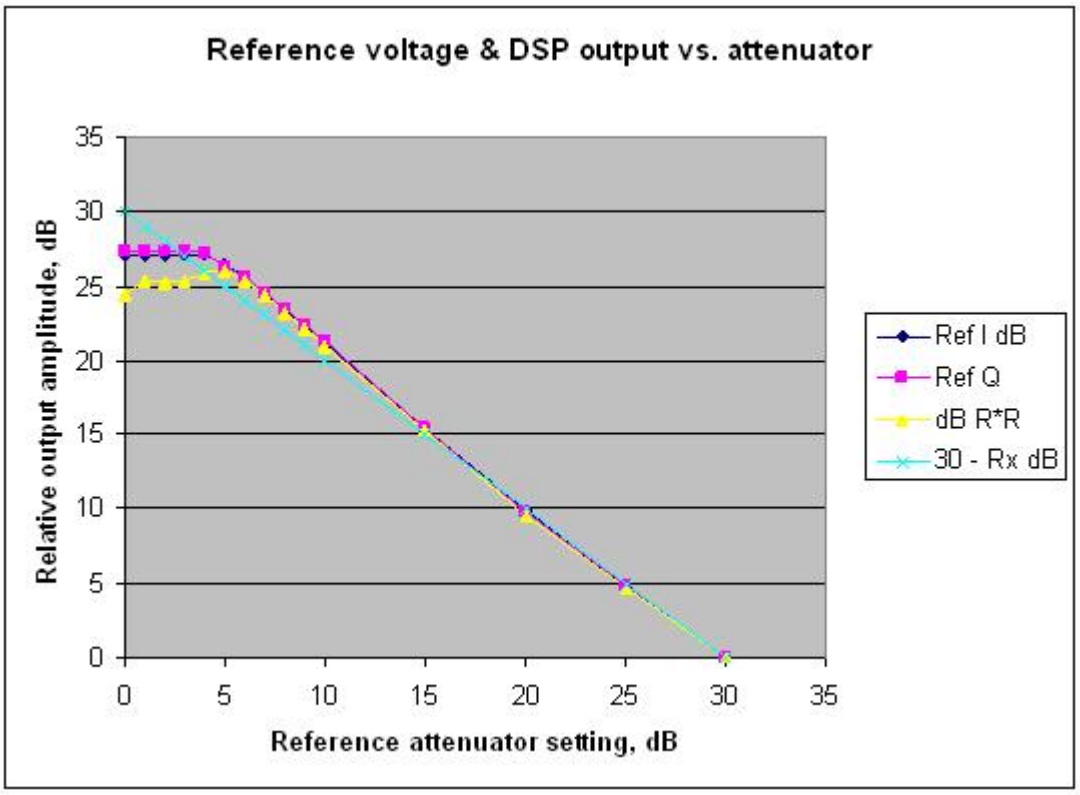

Figure 30: The values shown in Table 4 are plotted against the Reference Receiver attenuator settings. With this transmitter power, an attenuation of about 7 or 8 dB ensures linearity, which corresponds to a RefI and RefQ channel level of about 13 volts.

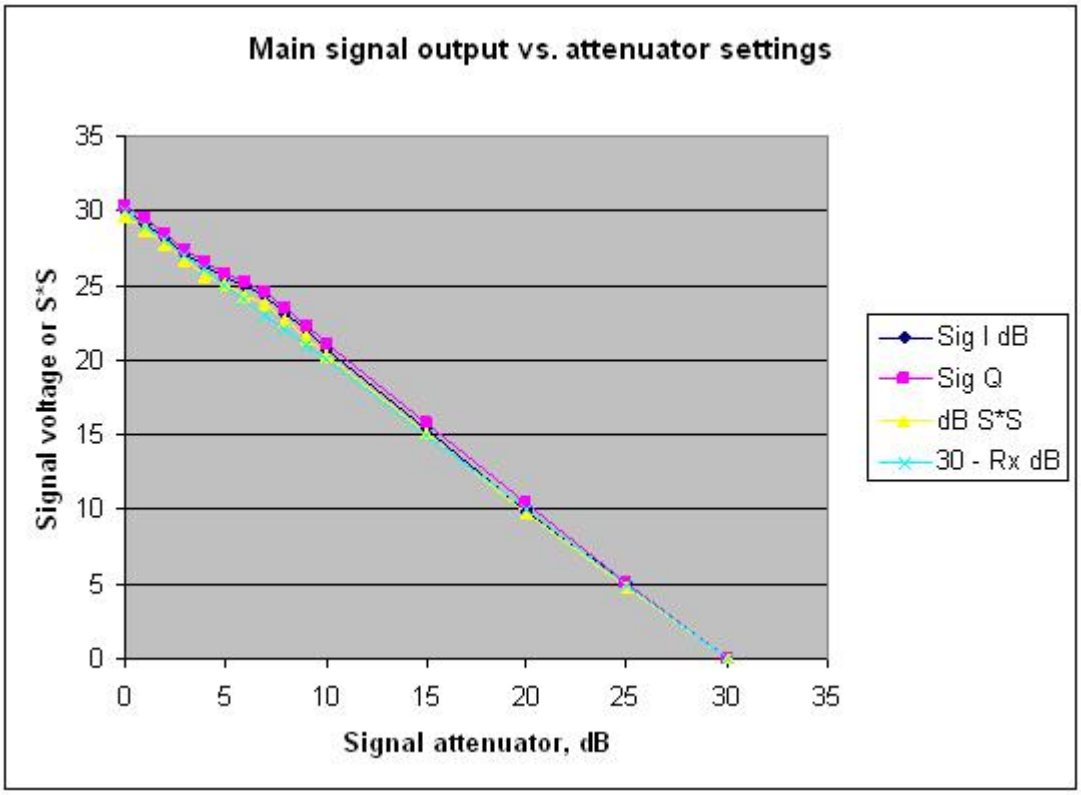

Figure 31: The values from Table 5 plotted against Main Signal attenuator settings. The deviation from linear seen between about 5 dB and 10 dB of attenuation is probably caused by a drift in the power output level of the transmitter.

Table 5: Holography Signal Receiver Linearity Measurements

Rx dB	Sig I	Sig Q	DSP S*S	dBSigI	dBSigQ	dB S*S	30 – RxdB
30	0.4	0.39	0.00014	0	0	0	0
25	0.72	0.7	0.00043	5.10545	5.080669	4.873404	5
20	1.25	1.29	0.00134	9.897	10.3905	9.809768	10
15	2.35	2.4	0.0045	15.38016	15.78293	15.07084	15
10	4.36	4.46	0.015	20.74853	21.16541	20.29963	20
9	5.06	5.1	0.02	22.04181	22.33011	21.54902	21
8	5.75	5.85	0.026	23.15216	23.52183	22.68845	22
7	6.55	6.6	0.033	24.28363	24.56959	23.72386	23
6	7.06	7.1	0.038	24.93489	25.20387	24.33656	24
5	7.55	7.64	0.045	25.51774	25.84058	25.07084	25
4	8.27	8.35	0.052	26.30891	26.61244	25.69875	26
3	9.05	9.19	0.065	27.09177	27.44502	26.66785	27
2	10.28	10.36	0.084	28.19866	28.4859	27.78151	28
1	11.46	11.65	0.105	29.14249	29.50523	28.75061	29
0	12.73	12.86	0.129	30.05537	30.36353	29.64462	30

D.2 Conclusion for Linearity After Attenuators

The optimum maximum level of input signal is with up to about 13 to 14 volts being indicated on the channel voltages with the antenna boresight on the transmitter. Too low a value may comprise s/n ratio, and two high a value may lead to receiver saturation. Depending on transmitter power output that might correspond to 0 to 1 dB on the Main Signal receiver, and about 4 to 10 dB of attenuation on the Reference receiver.

Note that, with a constant drive from the Transmitter Synthesizer, drifts with time of at least 6 dB in transmitter output power have been noted, so the above attenuation figures are just a guide. The Channel Voltages are the critical parameters.

D.3 Nonlinearity Before the Attenuators

The measurements shown above will not have detected any non-linearity that might occur before the attenuators in the receiver. The following measurements were made to put limits on any such non-linearity.

A constant pointing offset of the antenna was used to introduce a constant signal level change of about 1 dB into the receiver. The magnitude of this change at the output of the receiver was investigated while the absolute value of the input signal was varied over a range of about 20 dB. The 20 dB variation was introduced by varying the output power of the transmitter synthesizer, which drives a X6 multiplier. A 1 dB variation of the synthesizer produces very approximately 6 dB of change of transmitter output. Table 3 shows the measurements first of the Reference receiver, and secondly of the Main Signal receiver. A 2-degree offset in pointing created about 1.6 dB change in level at the Reference receiver, while a 25 arc second pointing offset produced a change of about 0.9 dB in the level to the Main Signal receiver. The results are plotted in Figure 32.

Table 6 lists measurements of the change in output power of both the Reference and the Main Signal receivers, for a fixed change of input signal. The change in output level, when the fixed change is inserted, is measured as a function of transmitter power level. The first two columns show the signal (R*R or S*S measured from the DSP Graph) measured on boresight and with the pointing offset, for different values, in dBm, of the

Table 6: Holography Signal Receiver Linearity Measurements

Reference		15 dB Attenuator Setting		
DSP R*R		Tx Synthesizer dBm		
Boresight	2 Degrees Off		dB Change	dB Boresight
0.018	0.0124	8	1.618508	-19.0658
0.05	0.034	9	1.674911	-14.6852
0.0052	0.0037	7	1.478016	-24.318
0.0013	0.00086	6	1.794449	-30.655
0.05	0.034	9	1.674911	-14.6852
Main Signal		10 dB Attenuator Setting		
DSP S*S		Tx Synthesizer dBm		
Boresight	25 arcsec off			
0.0162	0.013	9	0.955717	-18.8606
0.00535	0.0045	8	0.751413	-23.4679
0.0015	0.00125	7	0.791812	-29.0309
0.00039	0.0003	6	1.139434	-35.2288
0.000416	0.00034	6	0.876144	-34.6852
0.01625	0.0135	9	0.805196	-18.6967

Transmitter Synthesizer output. The ratio of boresight to offset pointing signal is calculated as "dB change" in dB, and plotted against boresight power in dB, calculated from column 1.

D.4 Conclusion for Linearity Before Attenuators

The plot of Figure 32 shows that, over a 20 dB range of output signal, an input step of respectively 0.9 or 1.6 dB produces the same step size in the output, to within about ±0.1 dB. There is no evidence of saturation of the input stages of the receiver at any level, with an upper limit of about 0.1 dB.

E Further Measurements of Pre-Attenuator Frontend Linearity

November 15, 2006 (DTE)

Using a similar technique, gain compression was looked for using a fixed antenna offset (35 arcsec in Azimuth for the main beam, 2 degrees for the reference beam) to give a switchable attenuation of the signal before the receiver of about −2 dB. For this measurement, the Agilent synthesizer was put at +13 dBm, and measurements were compared to an Agilent setting of +7 dBm. There is approximately 20 dB difference in output power between these two settings.

For each transmitter power setting, the attenuator in the respective receiver was adjusted to give about 9.5 volts IF channel voltage, according to the Settings panel of the Labview receiver control window. Using the DSP display, the ratio of powers at the on-beam and offset position was measured.

- *Main beam:*
  - **Measurement 1:**
    - Transmitter +13 dBm, Rx voltage 9.7 V, with attenuator at −24 dB.
    - Average of 4 measurements, on beam/35 arcsec offset, =1.76±0.06.

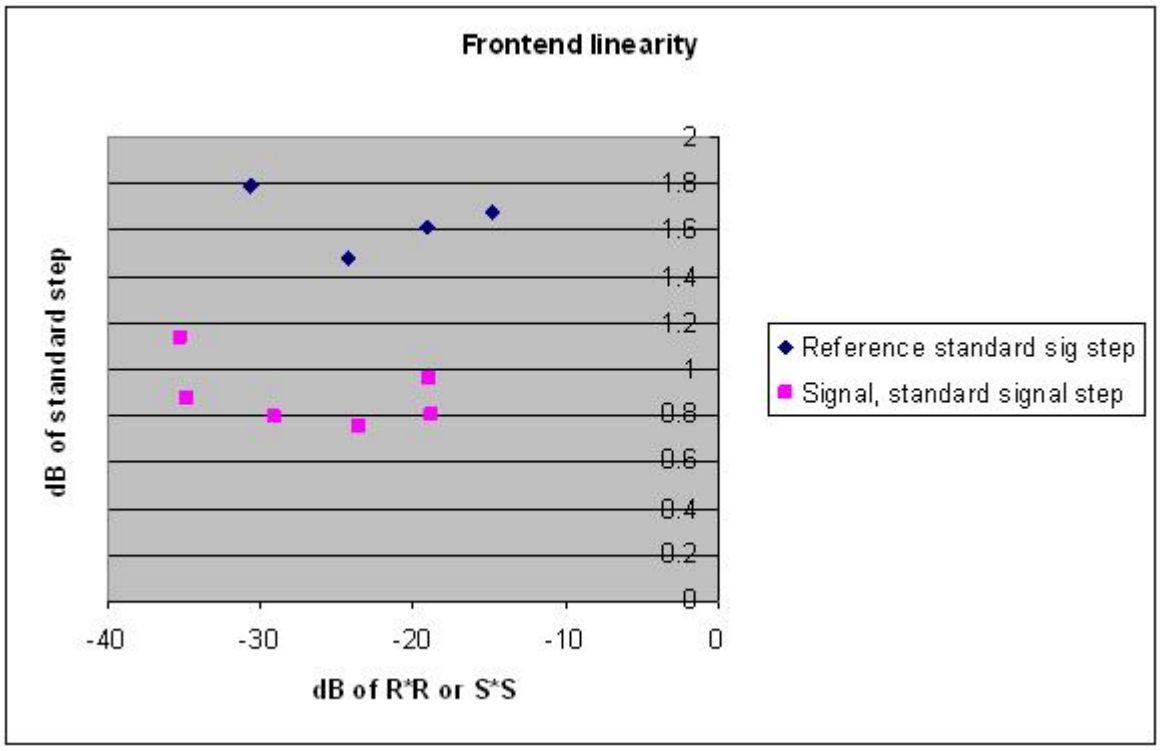

Figure 32: The change in output, in dB, for a fixed change in input signal, for the Reference and the Main Signal receivers.The input level was changed, by antenna pointing, by about 1.6 dB for the Reference receiver and by about 0.9 dB for the Main Signal receiver. The scatter is thought to result from drifts in transmitter output power during the measurements.

- **Measurement 2:**
  - Transmitter +7 dBm, Rx voltage 9.4V, attenuator −5 dB
  - Average of 3 measurements: ratio 1.743±0.025
- **Measurement 3:**
  - Transmitter +12 dBm, Rx voltage 8.9V, attenuator −17 dB
  - Average of 4 measurements: ratio 1.73±0.02.
- **Conclusion:** with the main beam, no gain compression is detected, with an upper limit of 3% at +13 dBm and an upper limit of 1% with +12 dBm.

— *Reference beam:*

- **Measurement 1:**
  - Transmitter +13 dBm, Rx voltage ∼ 9.5 V, attenuator −26 dB.
  - Average of 5 ratios: 1.51±0.03
- **Measurement 2:**
  - Transmitter +7 dBm, attenuator −11 dB
  - Average of 4 ratios: 1.47±0.05
- **Conclusion:** with the reference beam, no gain depression is detected, with an upper limit of about 3% at +13 dBm.

References

[Baars (1970)] Baars, J.W.M., "Dual-Beam Parabolic Antennae in Radio Astronomy", Dissertation Tech. Univ. Delft, 1970

[Baars (1983)] Baars, J.W.M., "Technology of Large Radiotelescopes for Millimeter and Submillimeter Wavelengths", in Infrared and Millimeter Waves, Vol. 9, p .241, Academic Press, 1983

[Baars *et al.* (1987)] Baars, J.W.M., Hooghoudt, B.G., Mezger, P.G. & de Jonge, M.J., "The IRAM 30-m Millimeter Radio Telescope on Pico Veleta, Spain", A&A, 175, p. 319, 1987

[Baars *et al.* (1994)] Baars, J.W.M., Greve A., Hein, H., Morris, D., Peñalver, J. & Thum, C., "Design Parameters and Measured Performance of the IRAM 30-m Millimeter Radio Telescope", Proc. IEEE **82**, p. 687, 1994

[Baars *et al.* (1999)] Baars, J.W.M., Martin, R.N., Mangum, J.G., MeMullin, J. &Peters,W.L.,"The Henrich Hertz Telescope and the Submillimeter Telescope Observatory", PASP, **111**, p. 627,1999

[Bennett *et al.* (1976)] Bennett,J.C., Anderson, A.P., McInnes, P.A. & Whittaker, A.J.T., "Microwave Holographic Metrology of Large Reflector Antennas", IEEE Trans. **AP-24**, p. 295, 1976

[Born & Wolf (1970)] Born, M. & Wolf, E., "Principles of Optics", Ch. 8, p. 370, Pergamon Press, 1970

[D'Addario (1982)] D'Addario, L. R. 1982, "Holographic Antenna Measurements: Further Technical Considerations", NRAO 12-Meter Telescope Memo 202. 1982

[Godwin *et al.* (1986)] Godwin, M.P., Schoessow, E.P. & Grahl, B.H., "Improvement of the Effelsberg 100 Meter Telescope Based on Holographic Reflector Surface Measurement", Astron. Astrophys. **167**, p. 390, 1986

[Greve (1986)] Greve, A., "Reflector Surface Measurements of the IRAM 30-m Radio Telescope", Int. J. Infrared and Millimeter Waves, **7**, p. 121, 1986

[Hachenberg *et al.* (1973)] Hachenberg,O., Grahl, B.H. & Wielebinski, R., "The 100-m Radio Telescope at Effelsberg", Proc. IEEE, **61**, p. 1288, 1973

[Hills *et al.* (2002)] Hills, R. *et al.* "High-Resolution Millimetre-Wave Holography on the James Clerk Maxwell Telescope", URSI Assembly Maastricht, 2002

[von Hoerner (1967)] von Hoerner, S., "Design of Large Steerable Antennas", AJ, **72**, p. 35, 1967

[Jennison (1966)] Jennison, R., "Radio Astronomy", 1966

[Lazareff *et al.* (2003)] Lazareff, B., Carter, M., Halleguen, S., Degoud,L., "Characterization of Holography Horns for ALMA Prototype Antennas", IRAM internal report, 2003

[Lucas *et al.* (2001)] Lucas, R., Glendenning, B. 2001, "ALMA Test Interferometer Raw Data Format", ALMA Software memo 15

[Moore (1982)] Moore, C. M. 1982, "Technical Considerations for Holographic Measurement of the NRAO 12-Meter Surface", NRAO 12-Meter Telescope Memo 174.

[Morris (1985)] Morris, D., "Phase Retrieval in the Radio Holography of Reflector Antennas and Radio Telescopes", IEEE Trans. **AP-33**, p. 749, 1985

[Morris (1988)] Morris, D., Baars, J.W.M., Hein, H., Steppe, H., Thum,C. & Wohlleben, R., "Radioholographic Reflector Measurement of the 30-m Millimeter Radio Telescope at 22 GHz With a Cosmic Signal Source", A&A **203**, p. 399, 1988

[Rusch & Potter (1970)] Rusch, W.V.T. &Potter, P.D., "Analysis of Reflector Antennas", Academic Press, 1970

[Ruze (1966)] Ruze, J., "Antenna Tolerance Theory", Proc. IEEE, **54**, p. 633, 1966

[Scott & Ryle (1977)] Scott, P. F. & Ryle, M. 1977, "A Rapid Method of Measuring the Figure of a Radio Telescope Reflector", MNRAS, 178, 539.

[Shepherd (2006)] Shepherd, D. S. 2006, "Software Documentation: ATF Operations.

[Silver (1949)] Silver, S., "Microwave Antenna Theory and Design", MIT Rad.Lab. Series Vol.12, 1949